Journal of Thermal Analysis and Calorimetry (2024) 149:1895–1933
https://doi.org/10.1007/s10973-023-12831-9

Different energy storage techniques: recent advancements, applications, limitations, and efficient utilization of sustainable energy

Raj Kumar[1] · Daeho Lee[1] · Ümit Ağbulut[2] · Sushil Kumar[3] · Sashank Thapa[4] · Abhishek Thakur[5] · R. D. Jilte[6] · C. Ahamed Saleel[7] · Saboor Shaik[8]

Received: 6 June 2023 / Accepted: 9 December 2023 / Published online: 27 January 2024

Abstract

In order to fulfill consumer demand, energy storage may provide flexible electricity generation and delivery. By 2030, the amount of energy storage needed will quadruple what it is today, necessitating the use of very specialized equipment and systems. Energy storage is a technology that stores energy for use in power generation, heating, and cooling applications at a later time using various methods and storage mediums. Through the storage of excess energy and subsequent usage when needed, energy storage technologies can assist in maintaining a balance between generation and demand. Energy storage technologies are anticipated to play a significant role in electricity generation in future grids, working in conjunction with distributed generation resources. The use of renewable energy sources, including solar, wind, marine, geothermal, and biomass, is expanding quickly across the globe. The primary methods of storing energy include hydro, mechanical, electrochemical, and magnetic systems. Thermal energy storage, electric energy storage, pumped hydroelectric storage, biological energy storage, compressed air system, super electrical magnetic energy storage, and photonic energy conversion systems are the main topics of this study, which also examines various energy storage materials and their methodologies. In the present work, the concepts of various energy storage techniques and the computation of storage capacities are discussed. Energy storage materials are essential for the utilization of renewable energy sources and play a major part in the economical, clean, and adaptable usage of energy. As a result, a broad variety of materials are used in energy storage, and they have been the focus of intense research and development as well as industrialization. This review article discusses the recent developments in energy storage techniques such as thermal, mechanical, electrical, biological, and chemical energy storage in terms of their utilization. The focus of the study has an emphasis on the solar-energy storage system, which is future of the energy technology. It has been found that with the current storage technology, the efficiency of the various solar collectors was found to be increased by 37% compared with conventional solar thermal collectors. This work will guide the researchers in making their decisions while considering the qualities, benefits, restrictions, costs, and environmental factors. As a result, the findings of this review study may be very beneficial to many different energy sector stakeholders.

Keywords Solar energy · Energy storage · Thermal energy storage · Mechanical energy storage · Biological energy storage · Chemical energy storage

✉ Daeho Lee
dhl@gachon.ac.kr

✉ Ümit Ağbulut
umitagbulut58@gmail.com

[1] Department of Mechanical Engineering, Gachon University, Seongnam 13120, South Korea

[2] Department of Mechanical Engineering, Mechanical Engineering Faculty, Yildiz Technical University, İstanbul, Turkey

[3] Department of Physics and Electronics, Hansraj College, University of Delhi, Delhi 110007, India

[4] Faculty of Engineering and Technology, Shoolini University, Solan, H.P 173229, India

[5] School of Physics and Materials Science, Shoolini University, Solan, H.P 173229, India

[6] Energy Centre, Maulana Azad National Institute of Technology (MANIT), Bhopal, M.P. 462003, India

[7] Department of Mechanical Engineering, College of Engineering, King Khalid University, PO Box 394, 61421 Abha, Saudi Arabia

[8] School of Mechanical Engineering, Vellore Institute of Technology, Vellore 632014, Tamil Nadu, India

Abbreviations

AP	Absorber plate
AES	Artificial energy storage
BES	Biological energy storage
CAS	Compressed air system
CES	Chemical energy storage
CNT	Carbon nanotubes
DP-SAH	Double-pass solar air heater
EES	Electrical energy storage
ES	Energy storage
ETC	Evacuated tube collector
FES	Flywheel energy storage
FPC	Flat-plate collector
FPSTC	Flat-plate solar thermal collector
HTF	Heat transfer fluid
HWS	Hot water system
MES	Mechanical energy storage
MFC	Microbial fuel cell
MP-SAH	Multi-pass solar air heater
PCM	Phase change materials
PD	Pressure drop
PDMS	Polydimethylsiloxane
PHS	Pumped hydroelectric storage
PV	Photovoltaic
PVDF	Polyvinylidene fluoride
RFB	Redox-flow batteries
SAH	Solar air heater
SE	Solar energy
SFPC	Solar flat-plate collector
SHM	Sensible heat materials
SHS	Sensible heat storage
LHS	Latent heat storage
PW	Paraffin wax
HT	Heat transfer
SMES	Superconducting magnetic energy storage
STC	Solar thermal collector
TEG	Triboelectric generator
TES	Thermal energy storage
TP	Thermal performance
UV	Ultraviolet
$\dot{m}$	Mass flow rate
Nu	Nusselt number
f	Friction factor
$\dot{m}$	Mass flow rate of air
η	Efficiency
η_t	Thermal efficiency
η_{exe}	Exergy efficiency

Introduction

Energy is a critical component of economic expansion and progress. Energy systems are dynamic and in a state of transition as a result of alternative energy sources, technical advancements, demand, costs, and environmental effects. Traditional energy production still relies on fossil fuels, but it has steadily shifted to new, innovative technologies that place a focus on renewable resources like solar and wind. The energy requirement has begun since the very early ages of human civilization on our planet. Humans have used wood and fire to cook food and for light purposes at night. With the constantly changing times, humans have learned to utilize other energy sources, such as solar and wind energy, for their multipurpose applications. Then, humans started to store the energy and convert it to another form when the sources of energy were limited. In the last few centuries, with the sudden increase in the world population and energy consumption, energy sources such as coal and petroleum were added to meet the needs of humans. The discovery of electricity played a substantial role in changing the entire scenario of energy usage. The old or conventional methods of energy were replaced by the invention and consumption of electricity. In the last few decades, other new energy sources, such as SE and nuclear energy, have also been identified as significant energy sources. The consumption of energy is increasing day by day, and according to a report, in 2019, the world's primary energy consumption was found to be around 1,57,064 TWh. In the same survey, it was pointed out that the continent of Africa consumed the least amount of energy (5367 TWh), while the Asia–Pacific (69,615 TWh) and North America (32,936 TWh) were the two regions with the highest energy consumption [1]. The current patterns pointed out that, with the increase in energy consumption, the requirement for energy storage systems will also be boosted in the upcoming years. According to the report of IRENA in 2017, the requirement for energy storage will increase almost three times by the year 2030. With a rise in energy consumption because of the rising population and increasing economy, there is a requirement to use renewable energy sources because their alternatives might be harmful to our ecosystem. The population is growing, the economy is developing, energy consumption per person is increasing, there is supply in remote areas, and there is supply in static forms for machines and portable gadgets. This is happening despite on-going price rises for energy. For the purpose of satisfying consumer demand, energy storage may provide flexible electricity generation and delivery. By 2030, the amount of energy that needs to be stored will treble from what it does now, necessitating the use of much more specialized equipment

and systems. SE is one of the best answers to the current predicament. There has already been a significant rise in the amount of work invested in creating solar technologies. A few of the major challenges that have arisen as a result of this process are reduced silicon cell efficiency, greater processing expenses, a lack of adequate infrastructure, and a qualified labor force [2]. Over the last 40 years, energy demand has increased almost proportionally with GDP (gross domestic product) growth. Since 1971, each 1% rise in worldwide GDP has been met by a 0.6% growth in primary energy consumption, likely to result in a yearly energy demand growth rate of roughly 2%. Simultaneously, there are serious signs showing that the energy-consuming approach should be drastically altered in the coming years [3, 4]. One sign seems to be that organic fuel sources (especially oil and gas) are depleted and therefore will run out in the coming years, and coal reserves will likewise run out sooner than many assume. The second indication is that the worldwide climate is becoming more sensitive to rising levels of energy demand, which leads to the creation of thermal waste as well as CO_2 as a result of the combustion of hydrocarbon fuel. Therefore, more and more debates emerge about whether total energy needs should be reduced despite population and economic development or if the causal connection between GDP and energy usage should be maintained [5, 6]. Renewable energy sources like the sun, air, and tides are becoming increasingly popular in this regard. Various possibilities depend on an H_2 economy, in which H_2 is produced as a main energy carrier by solar irradiation of H_2O and produces no pollutants other than H_2O [7, 8]. These renewable energy solutions, however, were still not financially effective with non-renewable fossil energy systems. Some other techniques of storage include artificial methods of converting SE into different forms that can then be stored and used on request. As per the physical principles employed for energy storage applications, artificial techniques are generally split into three broad classes. The first technique is based on the general characteristic of matter to undergo bulk heating, in which the amount of stored energy is equivalent to the material's specific heat capacity, resulting in sensible heat [9, 10]. The second way makes use of a characteristic of matter that allows it to absorb and release heat (latent heat) when it goes through phase transitions [11, 12]. Chemical reactions, the third approach, need energy to produce chemical molecules with large-energy chemical bonds that subsequently release their energy when disrupted [13]. For the supply of energy and meeting the demand for energy, energy storage systems play a very essential role. For the sustainable and renewable usage of energy, various energy storage methods such as TES, EES, PHS, BES, CAS, and SMES have been developed, and advancements have been made.

This review article provides an overview of the fundamental concepts behind the long-term storage and utilization of energy resources. In this article, various modes of energy storage, including TES, EES, MES, CES, and BES, as well as photonic energy conversion methods, are dissected in detail, along with the mechanisms behind them. In addition, pieces of literature about each of these various energy storage methods are offered. This study showed the recent advancements in energy storage systems and was extremely helpful for researchers working in the energy storage field. To offer greater insights into the distinctions, possible uses, and present state of all energy storage strategies, more comprehensive studies of all currently existing methods are required, which have been presented in this article. In order to help new researchers in this field, this review is a basic attempt to compile all the material currently available on all storage techniques produced to date. The article aims to address every important idea, covering its history, thorough categorization, present state, traits, and uses. This thorough collection will serve as a reliable source for upcoming advancements in this area. The majority of the relevant information has been compiled in this document, making it a useful resource for any future advancements pertaining to energy storage.

Energy storage techniques

In the last few decades, energy produced from distinct renewable sources has exhibited high progression and advancement. But the main problem with these kinds of sources is that they deliver an irregular supply of energy, which further makes it difficult to meet consumption demand. So, different energy storage techniques are utilized to solve this problem. In conventional energy storage systems, chemical energy storage-based lead batteries are used for storage purposes. There are various shortcomings in lead batteries. A large amount of energy cannot be stored in such a small volume. Consequently, a variety of new storage methods are being explored. Energy storage technologies are broadly classified into natural and artificial types.

Natural energy storage: photosynthesis

Photosynthesis is among the primary energy flows caused by the sun's radiation on the Earth's surface as shown in Fig. 1. Unlike different energy flows arising from SE, like air, terrestrial radiation, and water flow, photosynthesis seems to be the only method capable of long-term SE preservation in a natural manner [14, 15]. The amount of the photosynthetic energy flux, indicated as, may be computed using a simplified photosynthesis equation that explains the conversion of CO_2 and H_2O to glucose and O_2 [16], respectively, i.e.,

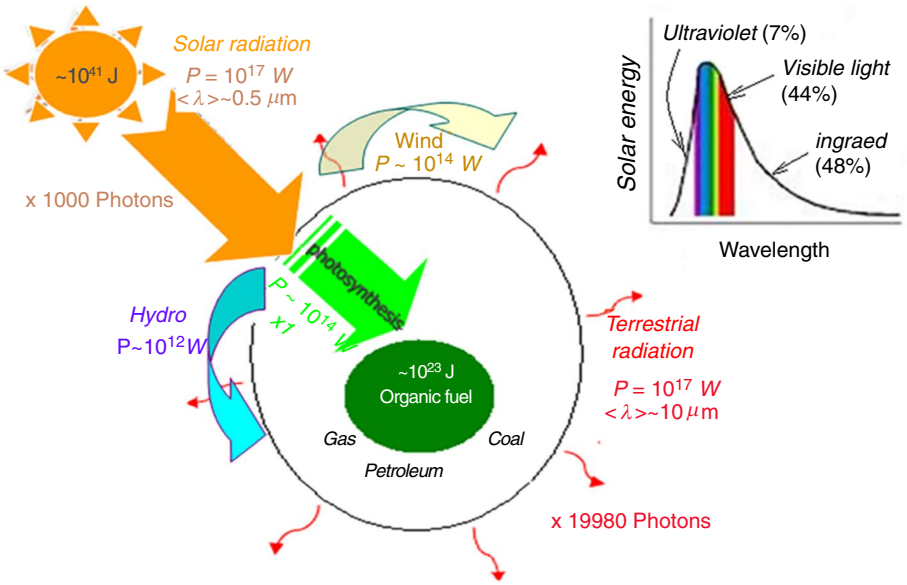

Fig. 1 Schematic diagram depicts the solar radiation spectrum at the earth surface [20]

$$CO_2 + H_2O \rightarrow CHOH + O_2 \tag{1}$$

The process explained by Eq. (1) includes the transmission of four electrons, each of which demands 1.2 eV of energy. As a result, the production of one O_2 molecule needs approximately 4.8 eV of energy. Moreover, the photosynthetic system's quantum efficiency is poor, requiring about ten red photons with an energy of approximately 2 eV to be absorbed, resulting in the production of one molecule of O_2. The amount of energy needed by photosynthetic systems to remove one molecule of carbon dioxide and create one molecule of oxygen is expected to be around $E_{O_2} + 10$ quanta + 2 eV = 20 eV. The free energy difference between newly formed carbohydrate bonds and the energy absorbed from carbon dioxide and water during the reaction results in a gain of roughly 465 kJ M^{-1} [17], resulting in an incredible conversion efficiency of approximately 23 percent. However, this value is significantly lower for a number of reasons, like the fact that a few photons are reflected or transmitted by canopy leaves, resulting in photon loss. Additional barriers to CO_2 fixation include the presence of water in leaves and suitable temperatures, both of which have an impact on the effectiveness of photosynthetic processes. Taking all limiting factors into account and considering all restricting factors, the best SE to biomass conversion efficiency is predicted to be 4.6% and 6% for C3 and C4 photosynthesis, respectively, at 30 ºC and 380 ppm (parts per million) of atmospheric CO_2 [18, 19]. Moreover, the average worldwide efficiency of photosynthesis has been predicted to be just 0.2–0.3 percent [17, 19].

It should be noted that without taking into account the limiting factors indicated above, the magnitude of global photosynthetic efficiency predicted above can always be achieved, but only by addressing worldwide photosynthetic oxygen production. The total oxygen generated by green plants per year is 10^{14} kg [21], which is similar to the mass rate of production of O_2.

$m_{O_2} = 3 \times 10^9 gs^{-1}$. The energy required to generate oxygen, as a result, will be

$$P_{O_2} = E_{O_2}\left(\frac{m_{O_2}}{M}\right)N_A = 1.8 \times 10^{14}\text{W} \tag{2}$$

The molar mass of oxygen, $M = 32$, is represented by N_A, the Avogadro constant. The amount of sun radiation that reaches the surface of the planet, i.e.,

$$P_{\text{Earth}} = P_{\text{Sun}} - \text{albedo} \sim 1.2 \times 10^{17}\text{W} \tag{3}$$

where albedo is assumed to be 28%, the average photosynthesis efficiency can be calculated as

$$\eta_{\text{org}} = \frac{P_{O_2}}{P_{\text{Earth}}} \sim 1.5 \times 10^{-3} \tag{4}$$

The relatively similar value for η_{org} can even be achieved using the expression

$$P_{\text{org}} = \eta_{\text{org}} S_{\text{Earth}} \times 230 \frac{W}{m^2} \tag{5}$$

Here, it is assumed that the plants contain the complete earth surface [22]. This conjecture actually appears to be fairly naive because there are enormous areas of ice, desert, or mountains that lack vegetation. From Eq. (4), the power efficiency can, however, differ regionally, relying mostly on growth scenarios of plant organisms, achieving up to 2% for extreme sugarcane farming in warm areas or for optimized algae farming in especially special pools. However, there are

some disadvantages to using photosynthesis as an energy storage method. The first disadvantage arises from the fact that photosynthesis consumes less than half of overall SE, resulting in a loss of nearly all UV and infrared radiation. Secondly, photosynthesis seems to have a low average efficiency, which is around two orders of magnitude smaller as compared to the efficiency of artificial photovoltaics like silicon solar cells. Moreover, photosynthesis should never be discounted in comparison with conventional non-renewable forms of energy (such as gas, oil, and coal), as the latter are derived from photosynthesis products and therefore represent an indirect way of consuming SE. As a result, from a worldwide perspective, the efficiency of converting SE to mechanical energy via the indirect method of burning organic photosynthesis products will be even lower, assuming that the burning process converts power efficiently to mechanical energy at a rate of about 40% that alone produces.

$$\eta_{\text{indir}} = 40\%\eta_{\text{org}} = 6 \times 10^{-2}\% \tag{6}$$

This result shows that the organic fuel reserves (gas, oil, and coal) are much more expensive forms of energy than the direct solar radiation itself.

Artificial energy storage

The storage technologies designed and developed by humans are termed artificial energy storage. They can be classified broadly based on the type of energy involved: TES, MES, EES, BES, and CES.

Thermal energy storage

In the TES technique, a material gains energy as its temperature rises and loses energy as the temperature drops. Utilizing this property enables the use of a range of materials with diverse thermal properties to produce a variety of results, which can result in various applications for TES. The fundamental assumption of all TES applications is the same. Energy is delivered to a storage system to be used and retrieved later. A cycle may be used to describe the process of storing thermal energy in three phases. The three stages are charging, storing, and discharging. The storage cycle applies to a variety of energy storage methods, including chemical, latent, and sensible storage. The main difference between these energy-storing techniques is the material type and operating temperature. TES involves LHS and SHS.

Latent heat storage (LHS)

LHS basically utilizes the phase transition of a material to store energy. Utilizing a solid-to-liquid phase transition, which is performed by solidifying and melting the substance, is the most popular technique. Heat is transmitted to the substance holding a significant quantity of heat throughout the melting process. When needed, the heat is released from storage, causing the substance to solidify once again. Phase change materials (PCMs) are most commonly known for storing latent heat. Water is the most widely known PCM that has been used since ancient times as ice for cold storage. PCMs are basically classified into two categories, i.e., organic and inorganic. Hydrocarbons, lipids, sugar alcohol, and paraffin wax are organic PCMs, whereas salt hydrates are classified as inorganic PCMs. Organic PCMs are chemically stable, safe, and non-reactive, but they have a low

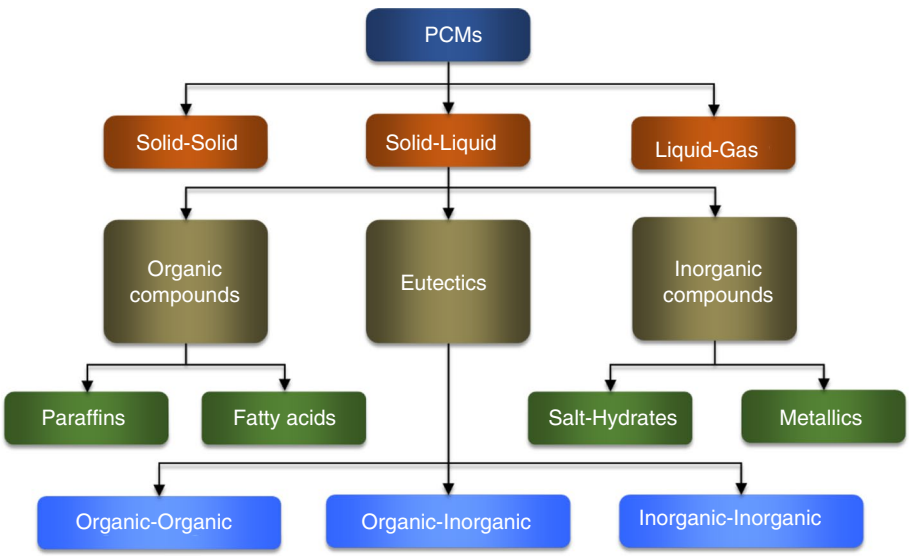

Fig. 2 Classification of PCMs

volumetric latent heat capacity. On the other hand, inorganic PCMs have a high heat of fusion and volumetric latent heat capacity, as well as a rapid melting point. The detailed classifications of the PCMs are shown in Fig. 2, and LHS performance enhancement techniques are illustrated in Fig. 3.

Zubair et al. [23] conducted an experiment to improve the performance of FPSC embedded with PCM. Two organic PCMs with distinct melting points, OM48 and OM-55, were inserted into the FPC riser tubers. The outcomes revealed that during the first phase with OM48, the η_t was increased by 14.5% and 15% in the first two days, whereas during phase 2 with OM55, the η_t was found to be enhanced by 16% and 11.5% in the next two days. Halim et al. [24] explored the TP of the STC by incorporating a PCM storage unit and also examined the effect of HTF on the TP. Underneath V-shaped APs, stearic acid was PCM. It was found that the TP of STC was 3.7% higher at 0.5 L min^{-1}, 9.9% higher at 1.0 L min^{-1}, and 11.3% higher at 1.5 L min^{-1} flow rate compared to the regular FPC that did not store PCM. The findings indicated that the utilization of PCM storage leads to efficiency enhancements in STC by 11.3% at 1.5 L min^{-1} of flowrate. Murali et al. [25] examined the performance of a thermosiphon hot water system integrated with a separate TES unit as depicted in Fig. 4. Paraffin wax was packed inside an aluminum tank to store thermal energy. The investigation of the charging and discharging efficiency of PCM was carried out. This finding demonstrates that the incorporation of 2.5 kg of PCM resulted in a maximum of 16% enhancement in the η_t.

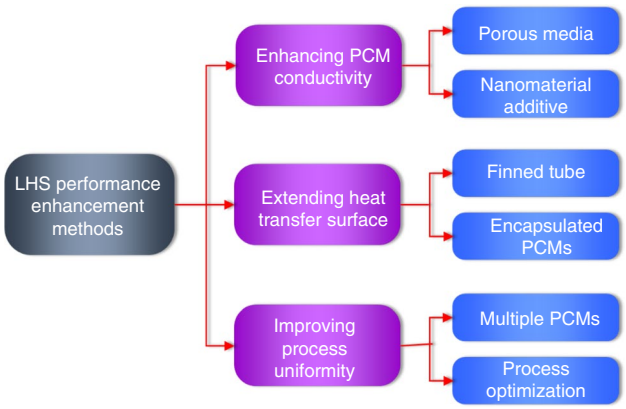

Fig. 3 LHS performance improvement techniques

Serale et al. [26] conducted a numerical examination of the TP enhancement of flat-plate STC embedded with slurry PCM. The results pointed out that instantaneous efficiency was found to be increased by 5–10% during the summer and by 20–40% during the winter season. Chopra et al. [27] led a thermal investigation of the ETC combined with PCM as shown in Fig. 5. SA-67 was used as a PCM in the developed system. To examine the TP of the system, the experiment was carried out at five different times (8, 12, 16, 20, and 24 l/h). The incorporation of SA-67 as a TES material led to a notable improvement in the η_t of ETC, with an increase ranging from 32 to 37%.

Felinski et al. [28] presented an investigational study to assess the consequences of PCM when combined with ETC as demonstrated in Fig. 6. Paraffin wax was fitted inside the ETC with a heat pipe. The outcomes revealed that the total useful heat of the ETC system was improved by 45–79% with PCM as compared to regular ETC.

Essa et al. [29] carried out an experimental analysis of the ETC's performance in conjunction with a PCM-integrated helical fin heat pipe as illustrated in Fig. 7. The study examined the effects of different $\dot{m}$ on the TP. The outcomes projected that the performance of ETC with helical heat pipe

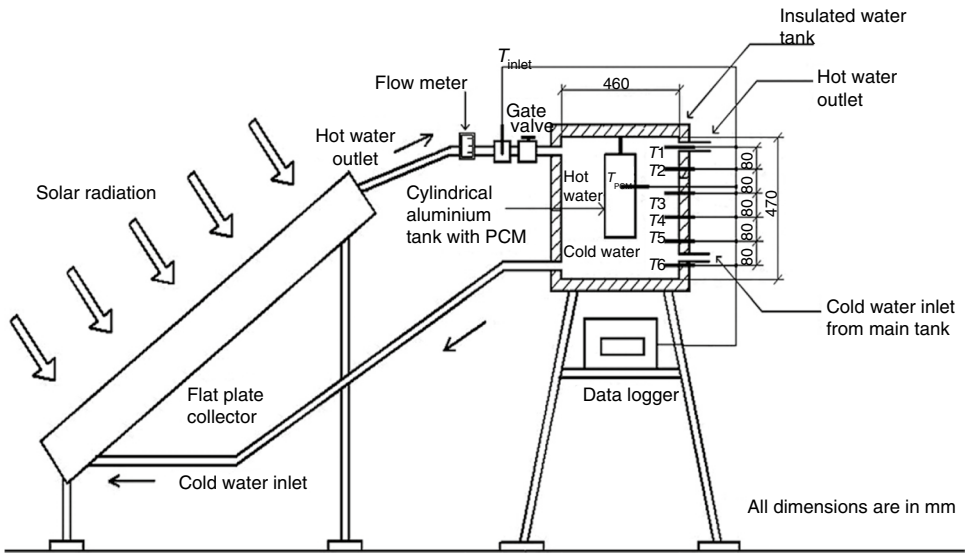

Fig. 4 Thermosiphon hot water system integrated with separate TES unit [25]

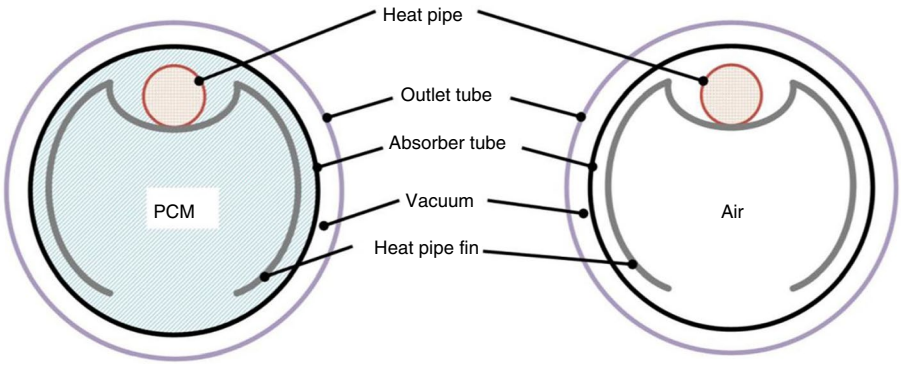

Fig. 5 Area of the cross-section of ET **a** with PCM **b** without PCM [27]

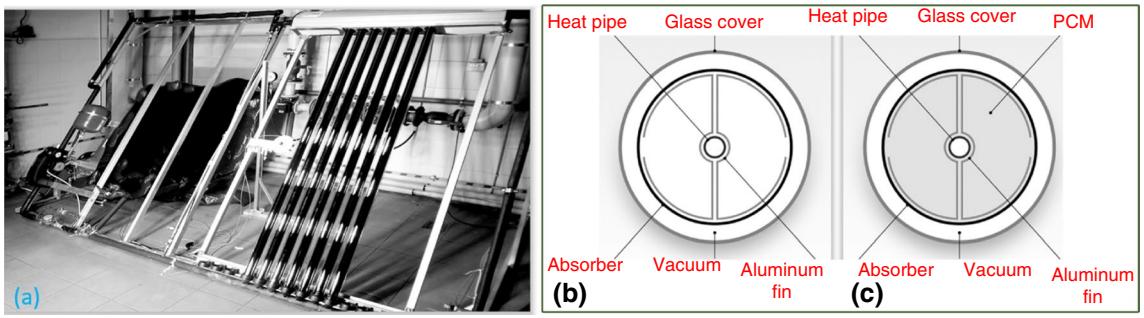

Fig. 6 Photographic presentation of setup and cross-sections of an ETC with a heat pipe (HP) inside **a** without PCM, **b** with PCM [28]

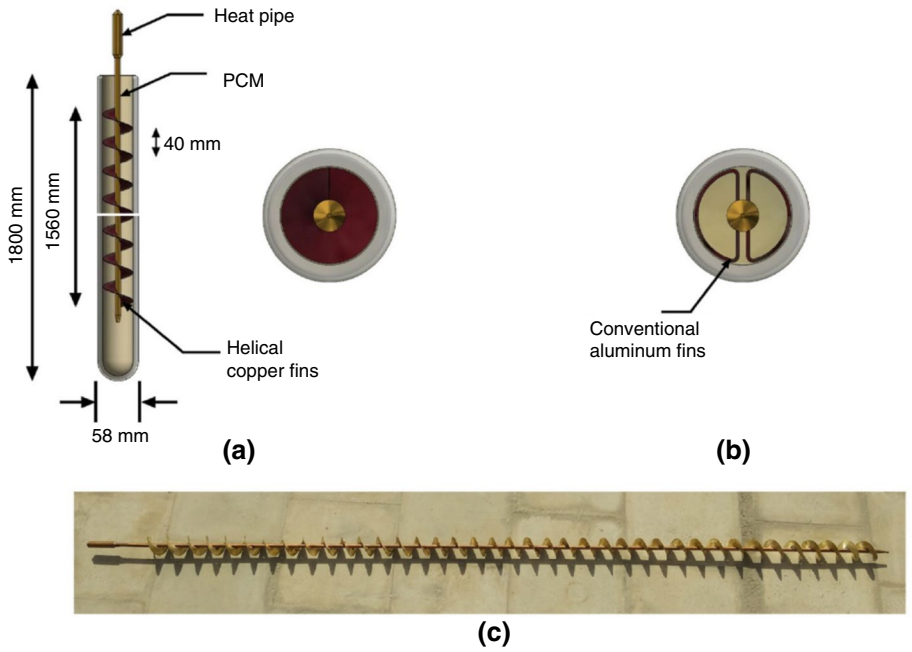

Fig. 7 Schematic illustration of PCM incorporated in HPETC with **a** helical fins, **b** conventional fins, **c** helical finned HP [29]

and PCM was found to be improved by 15% and 13.6% at 0.5 L min^{-1} and 0.665 L min^{-1}, of $\dot{m}$, respectively.

Mehla et al. [30] conducted a thermal investigation on the charging as well as discharging mechanisms of PCMs assimilated in evacuated tube SAH. The outcomes attained revealed that the system is more efficient at high $\dot{m}$ during charging and discharging of PCM, and a maximum average efficiency of 17.9% was attained at high $\dot{m}$ of 0.035 kg s^{-1}. Sudhakar et al. [31] performed an experimental examination on encapsulated PCM integrated in double-pass SAH as shown in Fig. 8. Paraffin wax was placed on the holes made in the AP. Three different formations or configurations

Fig. 8 Photographic view of FPC with PCM [31]

of APs were examined to assess their impact on collector performance. The outcomes of the experimental work show that the η_t of the collector with encapsulated PCM was 39%, whereas that of conventional FPC was only 31%.

Baig et al. [32] investigated the impact of the PCM incorporated with Al foam on the TP of DP-SAH. Four geometrical designs-conventional flat plate, Al foam with PCM inside two copper ducts, Al foam with PCM inside four copper ducts, and Al foam with PCM inside four copper ducts with pre-heat were studied. The results suggested that pre-heated Al foam with PCM inside four copper ducts was able to generate useful heat for 2.5 h after sunset, whereas Al foam with PCM inside two and four copper ducts was able to provide useful heat for 1.5 h after sundown. Sajawal et al. [33] performed experimentation on DP-SAH integrated with fin tube PCM, and thermal analysis was conducted. The discharging and charging characteristics of PCM were examined. Three various configurations-no PCM, RT44HC PCM inside the semi-circular finned tube, and RT44HC and RT18HC- two types of PCM inside finned tubes were explored. The findings showed that the DP-SAH maximum performance was achieved with the third configuration with RT44HC and RT18HC PCMs. The utilization of a PCM resulted in an increase in the average η_t of approximately 15%. Salil et al. [34] implemented an investigational study and calculated the η_t of DP-SAH when the PCM (paraffin wax) was placed on the heating plate as illustrated in Fig. 9. The influence of various $\dot{m}$ such as 0.6, 0.9, 1.2, and 1.8 kg min^{-1} and distinct solar irradiation (625, 725 and 825W m^{-2}) was scrutinized. The outcomes pointed out that a higher mass flow rate results in a delay in melting point.

Assadeg et al. [35] carried out the energy and exergy analysis of DP-SAH when integrated with PCM and fins. The influence of various $\dot{m}$ in the range of 0.01–0.15 kg s^{-1} and solar irradiations ranging from 425 W m^{-2}–1000W m^{-2} was analyzed. The results illustrated that an optimum energy efficiency of 73% was achieved at 0.15 kg s^{-1} of $\dot{m}$, and η_{exe} was found to be 2.5–4.2% when the solar radiation was maximum (1000W m^{-2}). Korti [36] performed a numerical simulation study on double-pass SAH with PCM media spheres as depicted in Fig. 10. The 2D model to conduct the simulations was developed. The examination was conducted on the influence of the inclusion of the PCM in the collector and the placement of the PCMs in different positions. The results revealed that the highest TP was attained when the PCM was positioned below the channel of SAH under the AP.

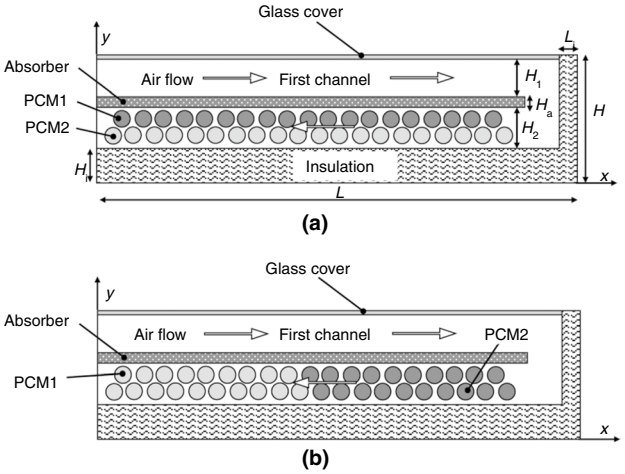

Fig. 10 Schematic of the DP-SAH design with two types of PCMs: **a** Parallel and **b** series. [36]

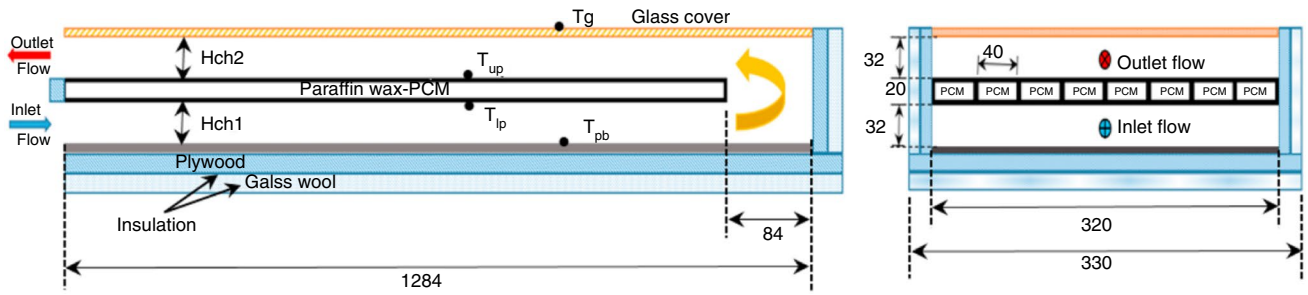

Fig. 9 Graphic diagram of DP-SAH integrated with PCM [34]

Ali et al. [37] examined the impact of the PCM on the TP of DP-SAH. Four altered configurations were studied: DP-SAH without PCM, PCM inside the copper tubes on the absorber, Al and steel rods inside the PCM used as thermal enhancers. The outcome showed that the maximum efficiency of DP-SAH of 96% was achieved with the third configuration (Al rod inside PCM). Singh et al. [38] directed an experiment to evaluate the HT characteristics of SAH having a distinct arrangement of the two APs integrated with PCM. The findings revealed that the highest air temperature difference at the inlet and outlet air of the collector with PCM in tubes was found to be 2–9 °C more as compared to the conventional SAH without PCM. The utilization of cylindrical tubes in conjunction with PCM resulted in an average η_t improvement of 22% compared to the utilization of a flat plate without PCM, at $\dot{m}$=0.03 kg s^{-1}. Srivastava et al. [39] presented a thermal analysis of recycled SP-SAH incorporated with TES medium. The design was made and fabricated, and the exergy analysis was conducted. The results revealed that the instantaneous η_{exe} was found to be 28.56%, whereas the average η_{exe} at night was 41.35%. Ameri et al. [40] inspected the thermal and heat transfer performance of V-corrugated SAH incorporated with PCMs. The investigation was carried out on the two types of PCMs (melting points 40° and 50°) with four different arrangements. The results illustrated that by using PCMs, the TP was enhanced from 53.1 to 62.6%. The η_t was enhanced by 9.5% as compared to SAH without PCM. The experimental findings also suggested that utilizing high-melting-point PCM enhanced the outlet temperature to about 5 °C. Wang et al. [41] conducted the experimental analysis of the TP of ETC with a lap joint-type flat micro-heat pipe and a separate TES system as demonstrated in Fig. 11. The experimental result of the TP was obtained at various values of flowrates and distinct weather conditions. The outcomes projected that the thermal storage efficiency achieved was in the range of 56.1–67.5% when the ambient temperature was in the range of 5.7–36.2 °C. The average thermal power extraction and thermal released efficiency both reached 1268 W and 98.5%, respectively.

Raj et al. [42] suggested a novel, efficient system to augment the TP of DP-SAH by using discrete macro-encapsulated PCM as shown in Fig. 12. The effect of different shapes of macro-encapsulated PCM (rectangular and cylindrical) on the TP of SAH was studied as demonstrated in Fig. 13. The findings indicated that the average encapsulated efficiency of cylindrical macro-encapsulated PCM obtained was 67%,

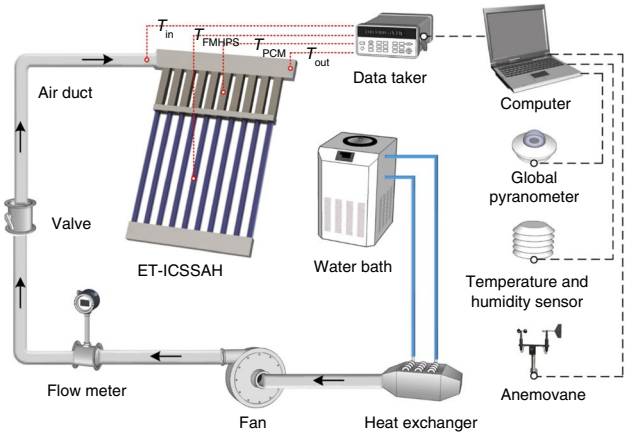

Fig. 11 Evacuated tube SAH integrated with PCM Tank [41]

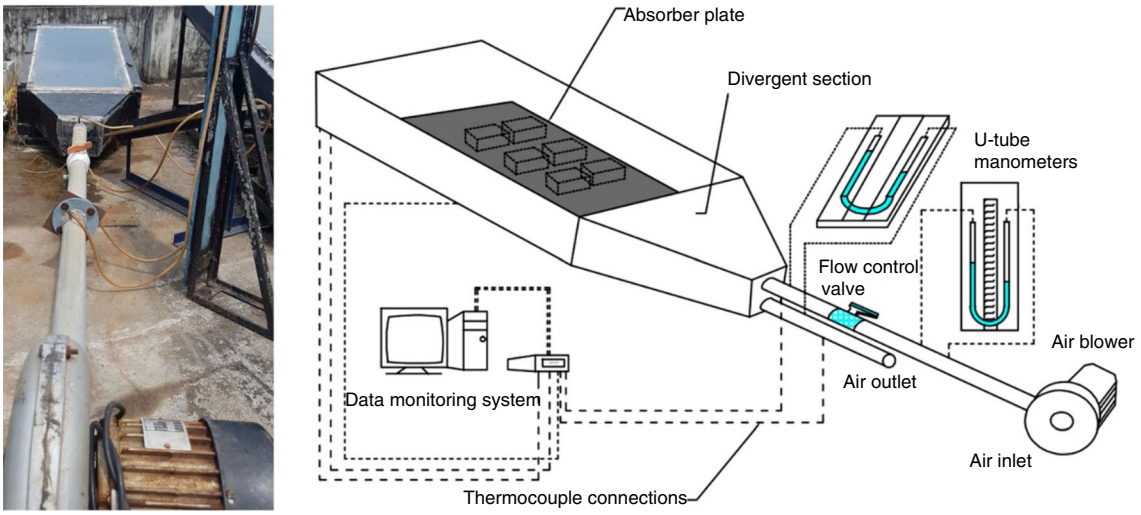

Fig. 12 **a** Pictorial view of DP-SAH and **b** schematic diagram of DP-SAH of setup [42]

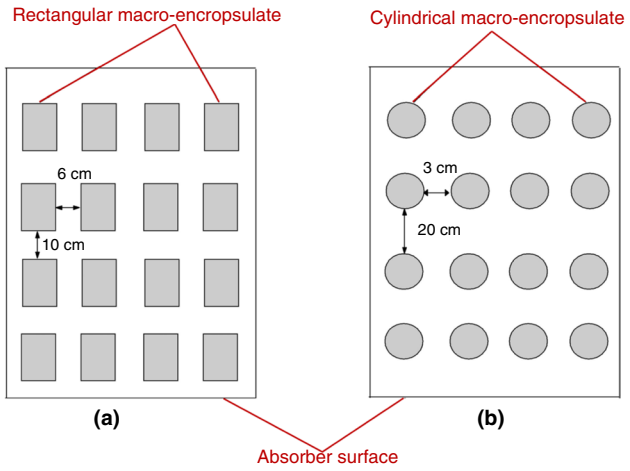

Fig. 13 Different shapes of macro-encapsulated PCM on AP [42]

whereas the efficiency was only 47% for rectangular macro-encapsulated PCM.

Moradi et al. [43] analyzed the TP of SAH with an energy storage medium (PCM) as shown in Fig. 14. The optimization of the SAH was carried out to obtain the maximum efficiency and highest air temperature difference at the inlet and outlet. The results pointed out that with 23 kg of paraffin wax as a 4-cm layer under the heating plate, the maximum temperature alteration achieved was 4.5 °C.

Wang et al. [44] examined the TP of SAHS incorporated with PCM based on a flat micro-heat pipe array as shown in Fig. 15. Lauric acid was used as the PCM in the setup. The experimental results pointed out two major outcomes: the high $\dot{m}$ of 240 m^3/h provided the maximum collector efficiency of 55% and the shortest charging time and slowest discharging time of PCM of 134 min and 154 min, respectively.

The thermophysical properties of various PCMs used to improve the performance of different solar thermal collectors (STCs) are given in Table 1, whereas the efficiency enhancement of the different STCs with various LHS mediums is summarized in Table 2. Figure 16 illustrates a comparison of the efficiency improvements of distinct STCs using various LHS mediums.

An examination of how various PCMs impact the performance of different types of solar collectors. The reason PCMs can store energy is because they capitalize on a material's phase change. When the material is melting, a large amount of heat is absorbed by it and is dispersed throughout the material. The material reverts to its solid form when the stored heat is eventually released. As an LHS medium, the review literature covers a variety of PCM types incorporated

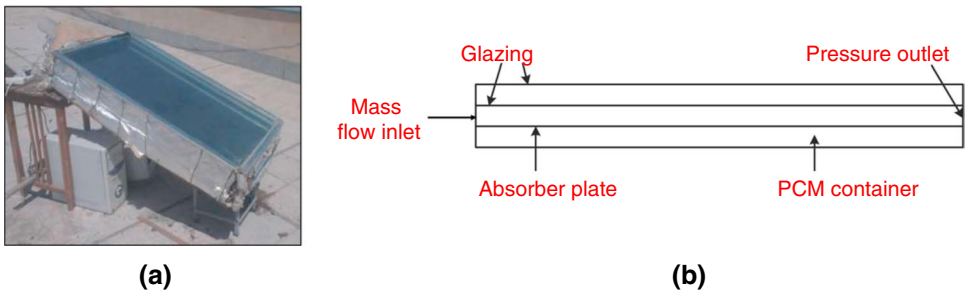

Fig. 14 **a** Schematic view of the SAH **and b** boundary conditions of the model [43]

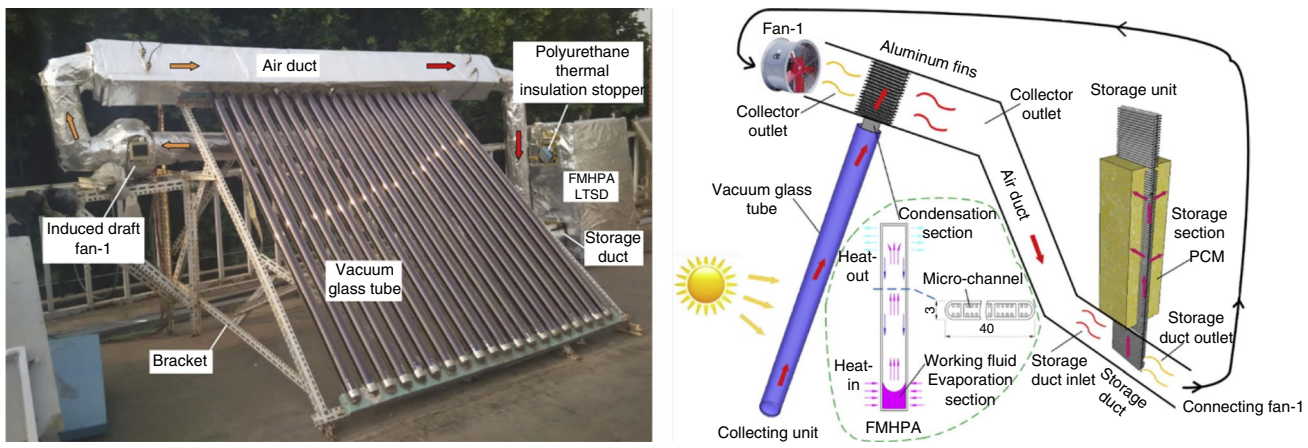

Fig. 15 Pictorial view of solar air collection-storage thermal system and its principle [44]

Table 1 Thermophysical properties of the studied PCMs with STCs

References	Material	$T_{melting}$/°C	H_{fusion}/kJ kg^{-1} °C^{-1}	C_p/kJ kg^{-1} K^{-1} or kJ kg^{-1} °C^{-1} or J kg^{-1} K^{-1}	
				Solid phase	Liquid phase
Murali et al. [25]	Paraffin wax (PW)	56 °C	142.7 (kJ kg^{-1})	2.4 (kJ kg^{-1} °C^{-1})	1.6 (kJ kg^{-1} °C)
Serale et al. [26]	Slurry PCM	37 °C	195	2025 J kg^{-1} K^{-1}	2025 j kg^{-1} K^{-1}
Chopra et al. [27]	SA-67	67.10 °C	244.21 (J g^{-1})	2.01 (kJ kg^{-1} K^{-1})	2.47 (kJ kg^{-1} K^{-1})
Felinski et al. [28]	PW	54.3 °C	–	1.8(kJ kg^{-1} K^{-1})	2.2 (kJ kg^{-1} K^{-1})
Mehla et al. [30]	Acetamide	80.85 °C	263 (kJ kg^{-1})	–	–
Sudhakar et al. [31]	PW	68.4 °C	102	2.1(kJ kg^{-1} °C^{-1})	2.1 (kJ kg^{-1} °C^{-1})
Sajawal et al. [33]	RT44HC & RT18HC two types of PCM	RT44HC = 41–44 °C RT18HC = 17–19 °C	250 & 260 (kJ kg^{-1})	2 (kJ kg^{-1} K^{-1})	2 (kJ kg^{-1} K^{-1})
Salil et al. [34]	PW	38–43 °C	174 (kJ kg^{-1})	2 (kJ kg^{-1} K^{-1})	2 (kJ kg^{-1} K^{-1})
Srivastava et al. [39]	PW	37–60 °C	214 (kJ kg^{-1})	–	–
Ameri et al. [40]	PW C16 & C30	40 °C, 50 °C	189 (kJ kg^{-1})	2 (kJ kg^{-1} K^{-1})	2 (kJ kg^{-1} K^{-1})

with various STCs. The results showed that the integration of the heat pipe ETC with SA-67 resulted in the highest η_t improvement of 37%.

Sensible heat storage (SHS) system

The SHS system includes raising the temperature of the storage material, which can be solid, liquid, or gas, to store heat. Sensible heat materials (SHMs) do not go through the phase transition of the material over the operating temperature range and basically store thermal energy in the form of sensible heat in the storage material. Solid materials such as porous media, rocks, concrete, pebbles, and ceramics, which have good thermal conductivity and are also available at a cheap price, can be used as SHS materials. Liquid materials such as engine oil, water, ethanol, and molten salts are also considered SHMs. The total energy stored in the material is the product of the mass, the heat capacity of the material, and the total change in temperature that the material goes through in this process. These are different techniques to store energy into different forms of energy, such as mechanical, electrical, and thermal energies [45]. Due to its widespread availability, low cost, and high specific heat value, water is the most popular and widely used SHS medium. However, the boiling point of water is 100 °C, so at temperatures higher than 100 °C, molten salt, oil, and other liquids are utilized. The detailed classification of the numerous types of SHS materials is given in Fig. 17. The thermophysical properties of different SHS materials are summarized in Table 3.

In most cases, sensible heat storage methods are utilized in combination with solar thermal applications operating at low temperatures. Because of its simple mechanism and affordable viability, a packed bed storage system (PBSS) is an ideal approach for TES. A basic PBSS has an insulated tank, storage material, a screen that serves to support the bed of packing pieces, and an inlet and outlet section. Storage elements are placed in a fixed bed as the SHS materials, in which thermal energy can be stored by raising the materials' temperature. In an effective PBSS, packing materials with high mass density are preferred in order to prevent thermal stratification. Air is commonly employed as an HTF in low-temperature solar thermal applications. The thermal energy that is collected by a solar collector is transferred to the storage material as the hot air from the collector travels through the bed. While discharging, the packed bed materials transfer the heat to the cold air flowing through the air channel. Figure 18 depicts the basic characteristics of an efficient PBSS. A photographic view of distinct types of SHS materials is shown in Fig. 19.

Mathew et al. [47] examined the evacuated tube heat pipe SAH integrated with the TES unit using η_t and η_{exe}, as shown in Fig. 20. The effect of four different $\dot{m}$(0.03, 0.1, 0.2, and 0.3 kg s^{-1}) on the TP was investigated. The greatest η_t and η_{exe} efficiency of 89% and 5.76%, respectively, were reached at 0.3 kg s^{-1} of $\dot{m}$, according to the results.

Kumar et al. [48] examined the TP of a multi-tabular SHS system (SAH) consisting of concrete incorporated with wire inserts as depicted in Fig. 21. The effect of the different parameters of wire inserts, such as pitch-to-diameter ratio, which varied from 0.5 to 1.0, was examined when the diameter of the wire inserts was 0.019 m. The outcomes pointed out that when the pitch-to-diameter ratio of the wire insert was 0.5, the extreme energy efficiency of the SHS system of 85.9% was achieved, whereas the maximum energy efficiency of conventional SAH without SHS was only 76.9%.

Kalaiarasi et al. [49] carried out an exergy and energy analysis of a flat-plat SAH incorporated with the SHS system as shown in Fig. 22. The AP and the tubes were made

Table 2 Efficiency enhancement of the different STCs with various LHS media

Author	Type of energy storage	Material type	Results
Zubair et al. [23]	LHS	OM48 and OM-55	Thermal efficiency (η_t) was increased by 14.5% and 15% in the first two days. During phase 2 with OM55, η_t was found to be enhanced by 16% and 11.5% in the next two days
Halim et al. [24]	LHS	Stearic acid	Utilization of PCM storage leads to efficiency enhancement in SWH by 11.3% at 1.5 L min^{-1} of flow rate
Murali et al. [25]	LHS	PW	The incorporation of 2.5 kg of PCM resulted in a maximum of 16% enhancement in the η_t
Serale et al. [26]	LHS	Slurry PCM	Instantaneous efficiency was found to be increased by 5–10% during summer and 20–40% in winter season
Chopra et al. [27]	LHS	SA-67	Thermal efficiency maximum improvement of 37.56% with PCM was achieved at the lowest 8 L/hr mass flow rate
Felinski et al. [28]	LHS	PW	The total useful heat of the ETC system was improved by 45–79% with PCM
Essa et al. [29]	LHS	PW	Thermal efficiency was found to be improved by 15% and 13.6% at 0.5 L min^{-1} and 0.665 L min^{-1} of $\dot{m}$ respectively
Mehla et al. [30]	LHS	Acetamide	Maximum average efficiency of 17.9% attained at high $\dot{m}$ of 0.035 kg s^{-1}
Sudhakar et al. [31]	LHS	PW	The efficiency of the collector with encapsulated PCM was 39% whereas the efficacy was found to be only 31% of conventional FPC. The η_t of the collector was improved by 8% as compared to traditional FPC
Baig et al. [32]	LHS	Al foam with PCM	Al foam with PCM inside four copper ducts is able to generate useful heat 2.5 h after sunset whereas Al foam with PCM inside two & four copper ducts is able to provide useful heat for 1.5 h after sunset
Sajawal et al. [33]	LHS	RT44HC & RT18HC are two types of PCM	DP-SAH maximum performance was achieved with the third configuration with RT44HC & RT18HC PCMs. The utilization of a PCM, resulted in an increase in the average η_t of approximately 15%
Salil et al. [34]	LHS	PW	Outcomes pointed out that a higher mass flow rate results in a delay in melting point
Assadeg et al. [35]	LHS	Silicon carbide	Optimum energy efficiency of 73% was achieved at 0.15 kg s^{-1} of airflow rate and η_{exe} was found to be 2.5–4.2% when the solar radiation was maximum (1000W m^{-2})
Korti [36]	LHS	Gravel, Dupont, and T23 PCMs	The highest TP was attained when the PCM was placed at the bottom of the absorbing plate
Ali et al. [37]	LHS	Paraffin wax	Maximum efficiency of DP-SAH of 96% was achieved with the third configuration (Al rod inside PCM)
Singh et al. [38]	LHS	PW	The utilization of cylindrical tubes in conjunction with PCM resulted in an average η_t improvement of 22% compared to the utilization of a flat plate without PCM, at $\dot{m}$ =0.03 kg s^{-1}
Srivastava et al. [39]	LHS	PW	The results revealed that the instantaneous η_{exe} was found to be 28.56% whereas the average η_{exe} at night was 41.35%
Ameri et al. [40]	LHS	Two different types of PW	Using PCMs, the thermal performance was enhanced from 53 to 62%. The η_t was enhanced by 9.5% as compared to η_t of SAH without PCM

up of copper, and Therminol-55 was packed inside the tubes to act as a SHS medium. The obtained results suggested that the energy efficiency was in the range of 49–59%, whereas the η_{exe} was in the range of 18–37%.

Jain et al. [50] assessed the enhancement of multi-pass SAH for paddy crop drying when integrated with an assembled thermal storage unit on a deep bed. The impact of parameters such as the area of the collector and the tilt angle of the collector was investigated. The day-to-day humidity

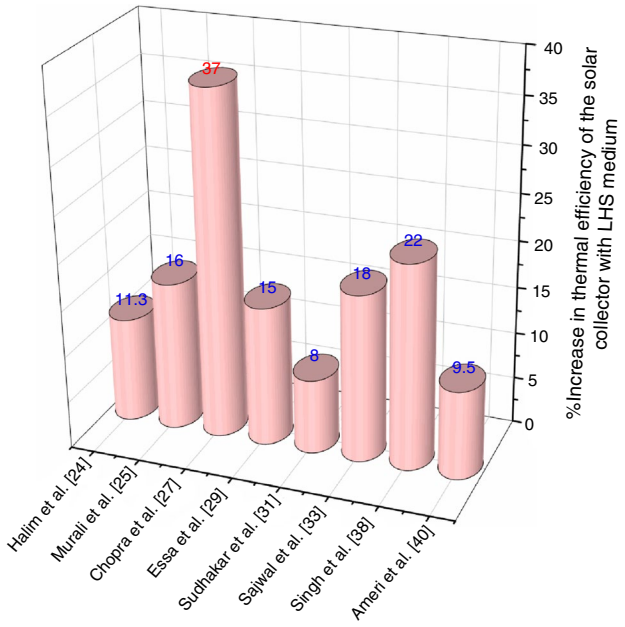

Fig. 16 Efficiency improvements of various STCs using different LHS media

and moisture evaporation of the exhaust air were analyzed. The outcomes revealed that the drying rate of the crop and air humidity rise as the drying bed depth increases. Jain et al. [51] directed the modeling of a reversed heating plate-type collector for a solar dryer incorporated with PBS. Analysis of crucial parameters such as airflow, channel width, and bed height was carried out. The obtained results show that 95 kg of onions with a moisture content of 6.14–0.27 kg water/kg was dried by SAH with a thermal storage for 24 h. Kareem et al. [52] examined the TP of the multi-pass (MP-SAH) combined with the SHS unit for drying Roselle. The experimental work was carried out under environmental conditions at 635W m^{-2} solar irradiance, 65% of relative humidity, 32 °C of surrounding temperature, and 0.81 m s^{-1} of wind speed. The results suggested that the collector and drying efficiency of MP-SAH with the SHS unit were found to be 70% and 64%, respectively. Jouybari et al. [53] investigated the impact of nanofluids and porous media-filled channels on the η_t of a FPSTC. SiO_2/water nanofluids with distinct volume fractions (0.2, 0.4, and 0.6%) are prepared, and their influence on STC with porous media is examined. The outcomes revealed that the efficiency of STC increased by 8.1%. Saedodin et al. [54] executed an experiment to examine the influence of porous metal foam on the TP augmentation of FPSTC as illustrated in Fig. 23. To determine the ideal porous material thickness and PD in the porous material of the FPSTC, a numerical analysis based on the thermal equilibrium postulate between fluid-porous material and the control volume approach was used. The attained

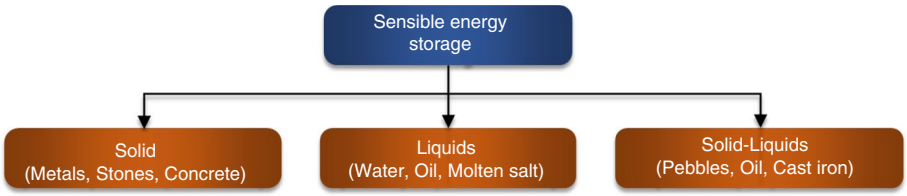

Fig. 17 Classification of SHS materials

Table 3 Thermophysical properties of distinct SHS materials

SHS material	State/phase of material	Range of temperature	Density/kg m^{-3}	Specific heat capacity/J kg^{-1} K^{-1}
Water	Liquid	0–100 °C	1000	4190
Pebbles Stone	Solid	–	1920	835
Ethanol	Organic liquid (OL)	0–78 °C	790	2400
Oil	Liquid	0–160 °C	888	1880
Rock	Solid	20 °C	2560	897
Propanol	OL	0–97 °C	800	2500
Glycerine	Liquid	17–290 °C	1260	2420
Bricks	Solid	200–800 °C	1600	840
Butanol	OL	0–188 °C	809	2400
Molten salt	Liquid	0–400 °C	1950	1570
Granite	Solid	–	2400	790
Octane	OL	0–126 °C	704	2400
Caloriea HT43	Liquid	12–260 °C	867	2200
Sand	Solid	200–300 °C	–	1.3
Concrete	Solid	200–400	1900–2300	850

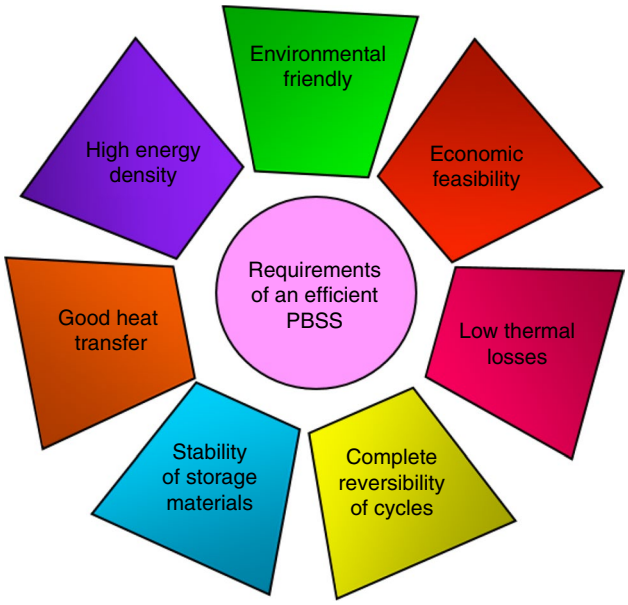

Fig. 18 Basic characteristics of an efficient PBSS

results concluded that porous media improved the η_t and *Nu* of the FPSTC up to 18.5% and 82%, respectively.

Hirasawa et al. [55] worked on the lessening of the heat losses in FPSTC by lessening the convection losses by using a porous medium. Above the collector's heating plate, a number of wire screens made of thin fishing lines were placed. The results indicated that 7% of the total reduction rate of convection loss from the FPSTC was achieved by using the high-porosity porous material. The η_t of the collector was enhanced by 7% as compared to conventional SAH. Kareem et al. [56] experimentally scrutinized the enactment of the SAH integrating with porous media. Porous media consists of the granite pebble bed. The porous materials lessened the heat losses during the nighttime, and the temperature variation between the ambient and exit air was 14.27 °C at 6:00 p.m. and 4.54 °C at 12:00 a.m. The obtained results proposed that the maximum η_t of 72% of SAH was achieved. Roy et al. [57] conducted a numerical analysis to assess the influence of porous media (wire mesh) on the thermal characteristics of DP-SAH as depicted in Fig. 24. The effect of distinct locations of the wire mesh (upper and bottom channels) at various flow rates and temperature differences at the inlet and outlet was studied. The results suggested that the highest temperature difference achieved was 62.4 °C at 0.0116 kg s^{-1}, and the lowest temperature difference attained was 42.7 °C at 0.0251 kg s^{-1}. The outcomes also showed that maximum DP-SAH efficiency of 82.2% was acquired at 0.0251 kg s^{-1} of $\dot{m}$ when the temperature difference was minimal.

Sopian et al. [58] directed a study to examine the η_t of DP-SAH with porous and non-porous media. The theoretic model of double-pass SAH was developed, and a comparative study between the experimental work and the theoretical model was carried out when the porous material was placed at different positions to augment the performance of HT. The influence of various factors, such as $\dot{m}$, rising temperatures, and solar irradiation, on the efficiency of DP-SAH was examined. The results showed that the placement of the porous media in the second channel enhanced the efficiency of the air heater by simply increasing the outlet temperature. The utilization of porous media in STC resulted in a 10% enhancement in efficiency compared to STC without porous media. Singh et al. [59] explored the influence of porous media containing wavy wire mesh on the thermal characteristics of single- and double-pass SAH as shown in Fig. 25. Findings from the experiments showed that η_t was 80% and the thermohydraulic efficiency of the DP-SAH was 74%. This was about 18% and 17% higher than the conventional SP-SAH.

Languri et al. [60] investigated the energy and exergy of DP-SAH with a porous medium added to the collector's bottom channel. The results of the experimental investigation pointed out that DP-SAH with a porous medium inside the bottom channel enhanced the η_t by 30% as compared to DP-SAH without the porous medium. Sopian et al. [61] carried out a study to analyze the η_t of DP-SAH with porous embedded inside the bottom channel of the collector. The significance of various factors, such as rising temperatures and solar radiation intensity, on the η_t of DP-SAH was examined. The outcomes showed that the placement of the porous media in the bottom channel improved the η_t of the SAH and increased the outlet temperature. Mahmood et al. [62] performed an experiment to determine the influence of wire mesh on the η_t of DP-SAH. The impact of significant factors such as solar intensity, $\dot{m}$, ambient temperature, outlet and inlet was examined. Omojaro et al. [63] investigated the TP and HT characteristics of steel wire mesh and fins in both SP-SAH and DP-SAH. The impact of the $\dot{m}$ range, which was 0.012–0.038 kg s^{-1}, on system performance was assessed. Also, the impact bed height in both the upper and lower channels was examined. The outcomes of the experiment showed that increasing the $\dot{m}$ results in enhancing the TP of both single and DP-SAH. The highest value of η_t for DP-SAH was determined to be 63.74%, whereas SP-SAH had a maximum value of 59.62%. Naphon et al. [64] evaluated the impact of the fin-embedded DP-SAH on HT characteristics and entropy generation. The $\dot{m}$ varied from 0.02 to 0.1 kg s^{-1}. The experimental outcomes concluded that the efficiency of the system increased as the height and number of fins increased, but entropy generation decreased with the increase in the number of fins. Murali et al. [65] conducted an experimental investigation on DP-SAH with fins embedded inside both the lower and upper channels. The various factors, such as inlet temperature,

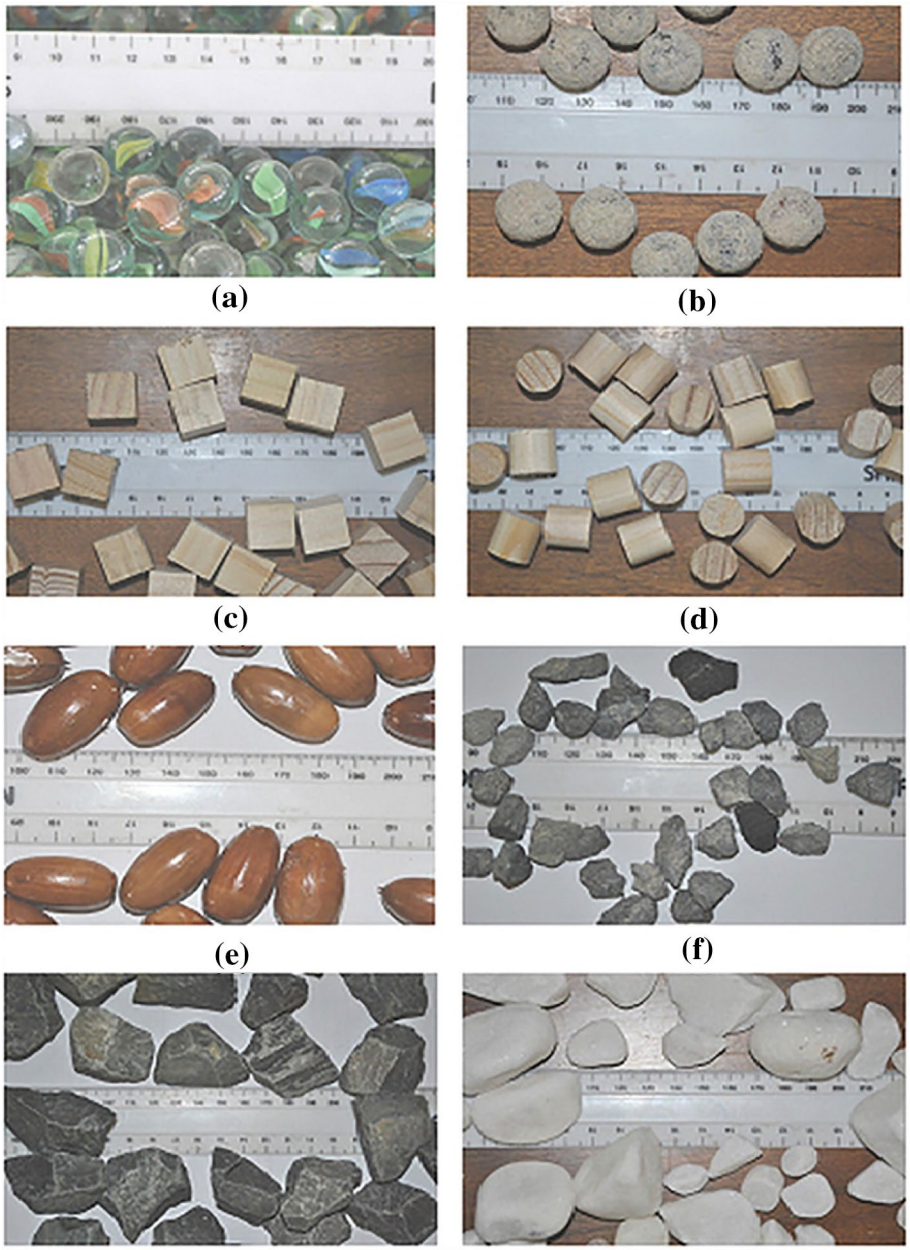

Fig. 19 Pictures of various packing elements: **a** smooth glass spheres, **b** sand-coated marbles, **c** wooden cubes, **d** wooden cylinders, **e** ellipsoids, **f** crushed rocks, and **g** rounded rocks [46]

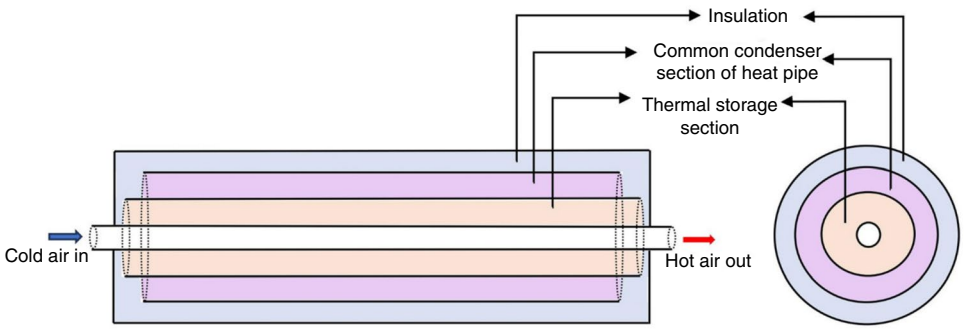

Fig. 20 Schematic view of TS-evacuated tube collector with heat pipe [47]

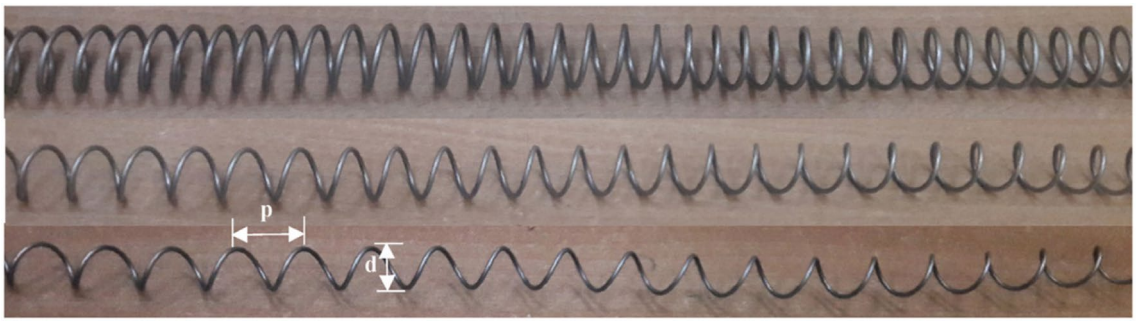

Fig. 21 Photographic view of wire coil inserts of different pitch ratios 0.5, 0.75, and 1 [48]

Fig. 22 **a** Integrated absorber cum SHS of SAH **b** SAH with an integrated copper tube for heat storage [49]

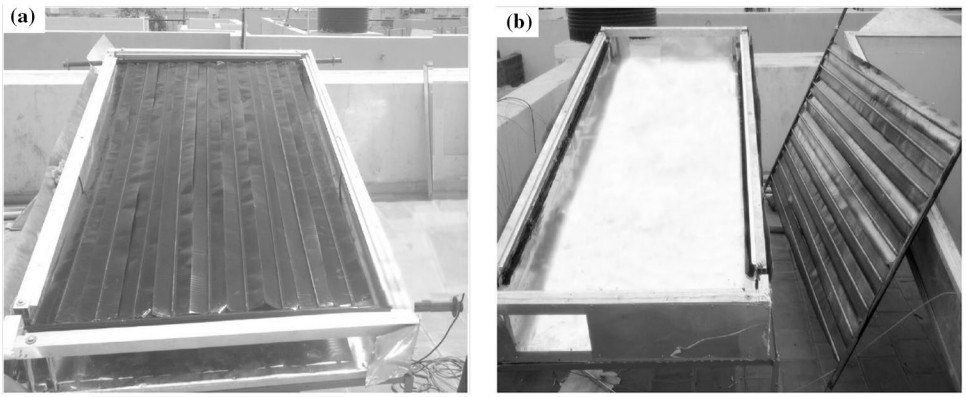

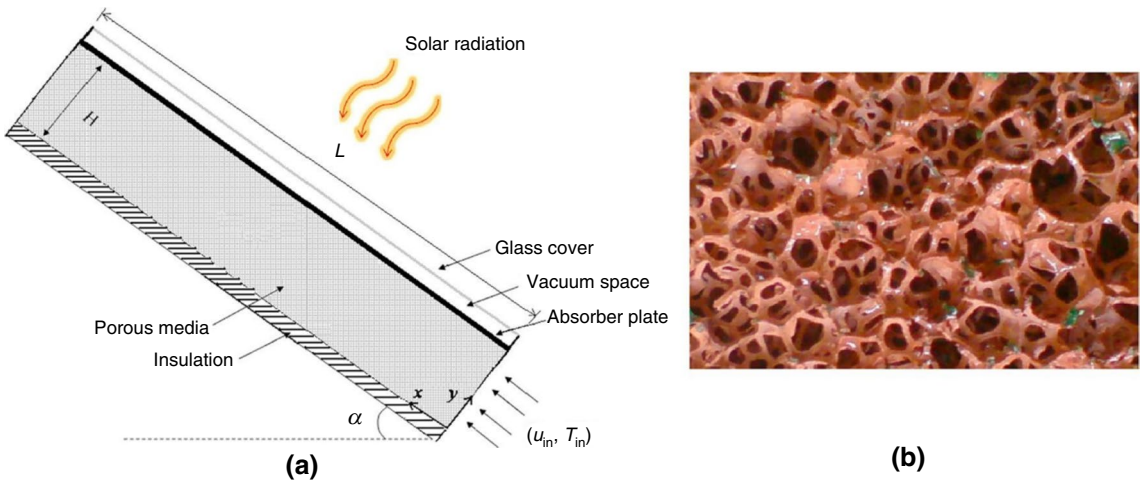

Fig. 23 **a** Schematic diagram of FPSTC with porous medium and its coordinates, **b** photographic view of copper metal foam [54]

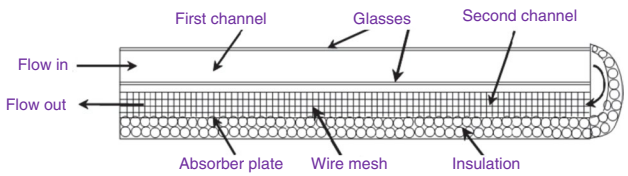

Fig. 24 Side view of DP-SAH integrated with steel wire mesh [57]

AP temperature, and outlet air temperature with and without rectangular fins, were examined. The impact of $\dot{m}$ was also evaluated. The outcomes disclosed that the η_t of the SAH when the fins are placed inside the lower channel is more productive or efficient as compared to the fins embedded inside the upper channel. Singh et al. [66] studied the thermohydraulic performance of the DP-SAH incorporated

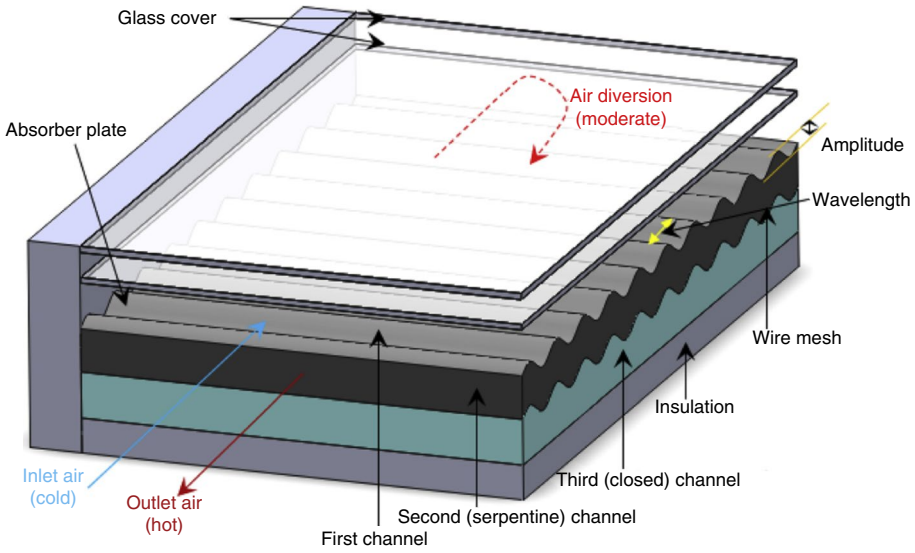

Fig. 25 Schematic diagram of SAH with porous serpentine wavy wire mesh [59]

with different types of fins (inline, staggered, and hybrid). The different geometrical parameters, such as fin angle ranging from 30 to 90°, fin height ranging from 0.007 to 0.0014 m, fin length varying from 0.007 to 0.0028 m, and three different types of fin arrangement, were investigated. Results showed that a collector with hybrid staggered fins had a thermohydraulic efficiency of 79%, which was 13% more efficient than collectors with inline and staggered fins. Agrawal et al. [67] worked on the assessment of the HT and f characteristics of PBSS incorporated with grooved cylinders. The schematic diagram and photographic view of the experimental setup are demonstrated in Figs. 26 and 27, respectively. The examination was conducted for four distinct types of heat storage elements: the first was a simple cylinder without a groove, and the other three were grooved cylinders. In the setup, the diameters of all the cylinders were kept constant, i.e., 100 mm, whereas the length of the storage elements was varied: 100 mm for the first solid cylinder and 100, 150, and 200 mm for the rest of the three grooved cylinders, respectively. The outcomes revealed that with the increase in the Reynold Number (Re), the Nusselt number (Nu) also enhanced and maximum Nu=518 was attained when the Re= 2050, aspect ratio (ϕ) = 1.0 and void fraction (ε) = 0.47.

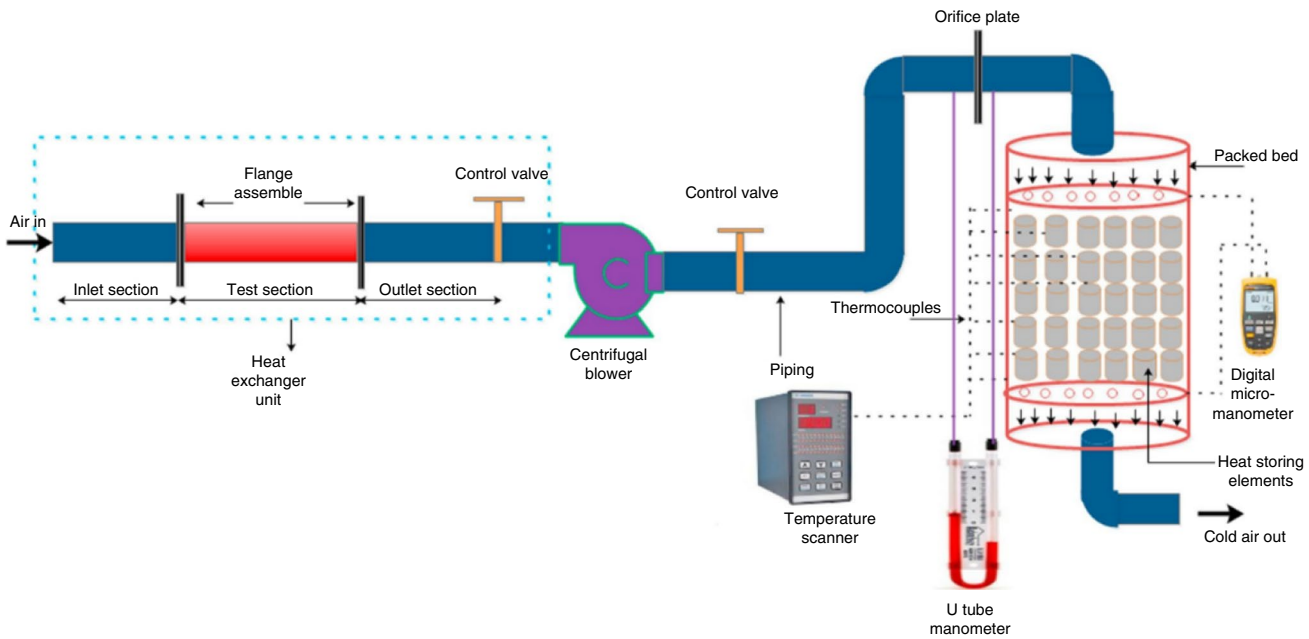

Fig. 26 Schematic diagram of the experimental setup [67]

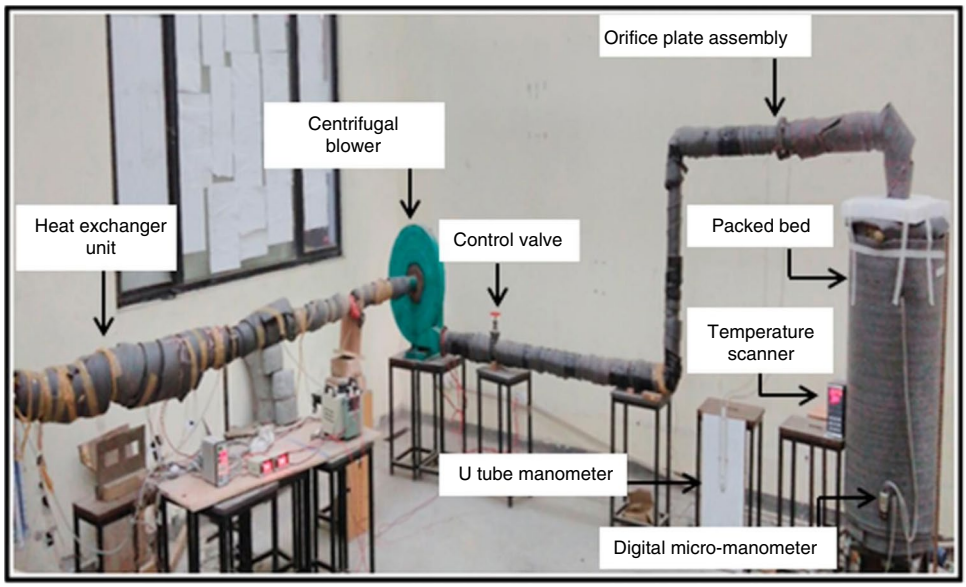

Fig. 27 Actual view of the experimental setup [67]

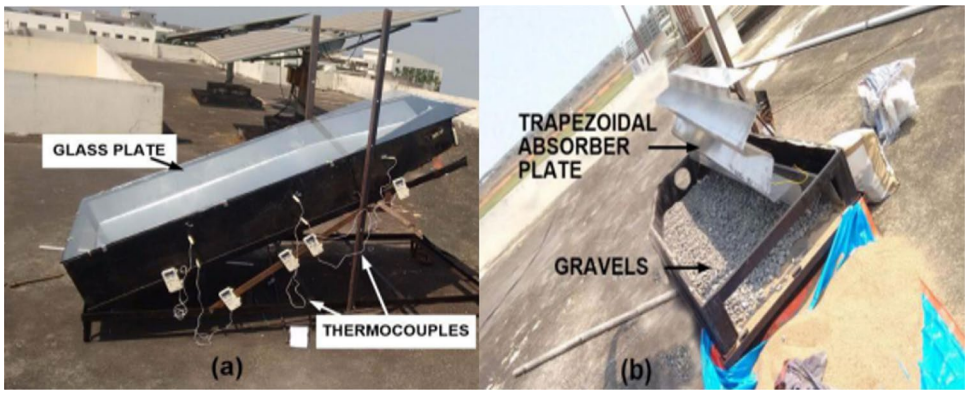

Fig. 28 **a** Photographic view of the experimental setup **and b** photographic view of the trapezoidal corrugated heating plate and gravels [68]

Lakshmi et al. [68] performed an energy and exergy analysis of SAH using SHS material and an AP that was corrugated in the shape of a trapezoid as depicted in Fig. 28. The SHS material that is utilized is gravel, and it is put underneath the AP. SAH's TP is analyzed and contrasted with flat- plate SAH, both with and without SHS materials. The values of solar radiation intensity, temperatures at different SAH locations, daily thermal, and η_{exe} are computed. Whereas the average daily η_t of a trapezoidal corrugated absorber with SHS material is 36.6%, the average daily η_t of a flat-plate SAH with corrugated sheets is 8.5% and 12.2%, respectively. The highest η_{exe} obtained using a trapezoidal corrugated absorber made of SHS material is 12.56%.

Koekemoer et al. [69] investigated the influence of distinct types of materials and their particle sizes on the PD of a packed bed STC. The Ergun equation was utilized to determine the PD across the packed bed. In the experimental study, the Ergun equation was extended for packed bed STC with three different types of large particles, such as coal, char, and ash particles. A schematic diagram of PD and void age measurement test unit is shown in Fig. 29. The outcomes suggested that the newly developed Ergun equation, with the assistance of regression analysis, had a better value for the estimated pressure drop of coal, char, and ash than the usual Ergun equation.

Halkarni et al. [70] examined the impact of inserts placed across the packed beds in this study. At the entry of a packed bed, the impact of a flow condition on the PD is studied. A schematic diagram of the setup for the PD measurements in a packed bed of spheres is illustrated in Fig. 30. Because of the channeling effect, the distribution of inserts reduces the PD in packed beds (increase in void fraction). The PD characteristics are unaffected by disturbed flow in the upstream zone of a packed bed with or without inserts.

The efficiency enhancements of the different STCs with various SHS mediums are summarized in Table 4. The comparison of efficiency enhancement of the different types of STCs with different SHS mediums is given in Fig. 31.

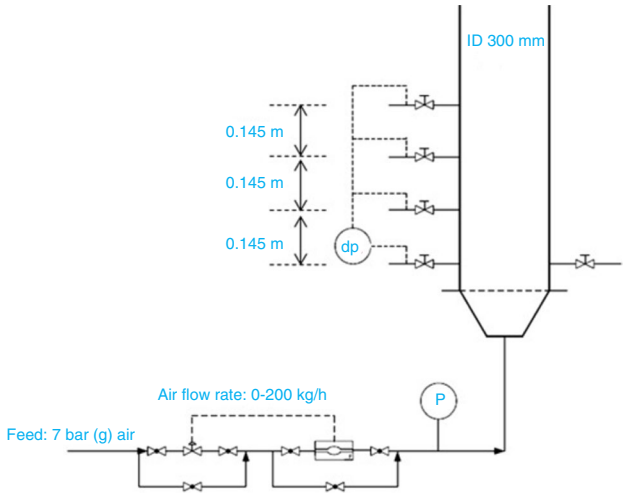

Fig. 29 Schematic diagram of PD and void age measurement test unit [69]

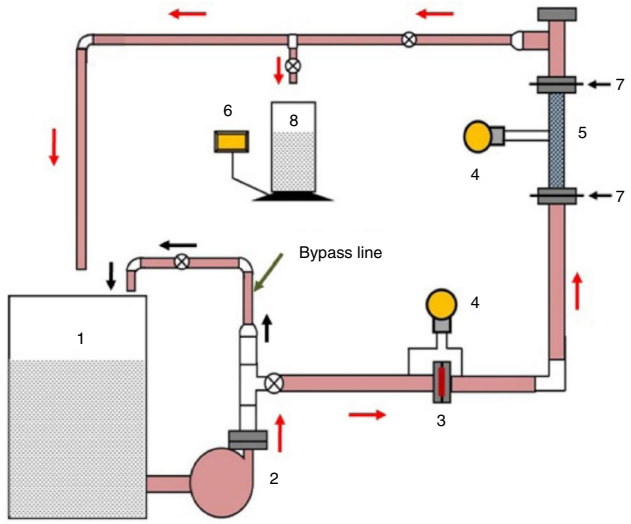

(1) Water reservoir (2) Centrifugal pump (3) Orifice plate (4) Differential pressure transmitter (5) Test section (6) Platform scale (7) Wire mesh (8) Measuring tank

Fig. 30 Schematic diagram of the setup for the PD measurements in a packed bed of spheres [70]

It was discovered from the literature discussed above that different kinds of SHS media are incorporated in different STCs. Comparing the results with traditional solar thermal collectors, it was found that DP-SAH embedded with porous medium utilized as SHS medium obtained the greatest η_t improvement of 30%.

Mechanical energy storage (MES)

In recent decades, the MES system has become one of the most sustainable and effective types of energy storage systems. MES systems are basically classified into three types: PHS, CAS, and FES, as shown in Fig. 32. Mechanical springs, gravity, and liquid pistons are some of the other methods of MES systems. The most important consideration in selecting the best system among these depends on certain factors, such as available space, energy source, and load nature. It is also worth noting that the various varieties of MES systems share some common benefits, such as a relatively quick response time and no negative environmental consequences. MES systems are appealing because they have several advantages over conventional energy storage systems, particularly in terms of environmental effect, cost, and long-term viability.

Flywheel energy storage (FES)

Flywheels have been used since ancient times, but only in recent decades have they been recognized as a form of bulk energy storage. The FES system stores energy in the form of kinetic energy for a short period by utilizing rotating mass, as shown in Eq. (7). Flywheels are the most efficient energy storage systems in terms of quick response time while also being cost-efficient. FES systems have various applications that are used in various sectors, such as railways, marine, hybrid automobiles, and wind power systems. There are basically four shapes of flywheels, i.e., thin and thick rings, solid disks, and disks of level. Each flywheel is described by a shape factor (K), demonstrating the use of material. The amount of stored specific energy per unit of mass is proportional to shape factor K, as shown in Eq. (8). Different types of flywheels and their components are shown in Figs. 33 and 34, respectively.

$$E = \frac{1}{2} I w^2 \tag{7}$$

$$\frac{E}{m} = K \frac{\sigma_{\mathrm{MAX}}}{\dot{\rho}} \tag{8}$$

Pumped hydroelectric storage (PHS)

Pumped hydroelectric storage is a MES system that is flexible, has a long-life cycle, and requires very little maintenance. This type of MES system consists of three main components, i.e., the upper reservoir, hydro-turbine, and pumping system. The PHS system also has a lower reservoir that pumps water to the upper reservoir when there is additional energy; it can be used again when required. The PHS system relies on potential gravitational energy. The upper reservoir delivers the positive pressure difference with respect to the lower reservoir and, subsequently, produces

Table 4 Efficiency enhancement of the different STCs with various SHS mediums

Author	Type of energy storage	Material type	Results
Mathew et al. [47]	SHS	Therminol- 55	Maximum η_t of 89% was obtained at 0.3 kg s^{-1} of $\dot{m}$ and energy efficiency was 5.76% respectively at 0.3 kg s^{-1} of $\dot{m}$
Kumar et al. [48]	SHS	Concrete with wire inserts	Maximum energy efficiency of the SHS system of 85.9% was achieved
Kalaiarasi et al. [49]	SHS	Therminol- 55	Energy efficiency was in the range of 49–59% and η_{exe} was in the range of 18–37%
Jain et al. [50]	SHS	Deep bed	With increase in the depth of the drying bed, the drying rate of the crop and humidity of air also enhances
Jain et al. [51]	SHS	Packed bed	SAH with thermal storage dried 95 kg of onion in 24 h having a moisture content of 6.14–0.27 kg water/kg
Kareem et al. [52]	SHS	Granite	The drying efficiency of MP-SAH with SHS unit was found to be 70% & 64% respectively
Jouybari et al. [53]	SHS	Porous metal Foam	The thermal efficiency of STC was found to be increased by 8.1%
Saedodin et al. [54]	SHS	Porous metal Foam	Thermal efficiency was improved by 18.5% Nu also enhanced up to 82%
Hirasawa et al. [55]	SHS	High-porosity Nylon fishing lines	The collector was enhanced by 7% as compared to conventional SAH
Kareem et al. [56]	SHS	Granite pebble bed	Maximum η_t of 72% of MP-SAH achieved
Roy et al. [57]	SHS	Wire mesh	The highest temperature difference achieved was 62.4 °C at 0.0116 kg s^{-1} and the lowest temperature difference attained was 42.7 °C at 0.0251 kg s^{-1}
Sopian et al. [58]	SHS	Porous material	The utilization of porous media in STC resulted in a 10% enhancement in efficiency compared to STC without porous media
Singh et al. [59]	SHS	Wavy wire mesh	Thermal efficiency was found to be 80% and thermohydraulic efficiency achieved was 74% which was approximately 18% & 17% more as compared to the conventional SP-SAH
Languri et al. [60]	SHS	Porous material	DP-SAH with a porous medium inside the bottom channel enhances the η_t and obtained η_t was 30% more as compared to DP-SAH without a porous medium
Sopian et al. [61]	SHS	Porous material	Placement of the porous media in the bottom channel improves the η_t of the SAH and the increase in the outlet temperature
Mahmood et al. [62]	SHS	Wire mesh	As the $\dot{m}$ was increased, the η_t of the system was also enhanced and was found to be a maximum value of 86% at 0.018 kg s^{-1}
Omojaro et al. [63]	SHS	Fins and steel wire mesh	Increase the $\dot{m}$ results in enhancing the thermal performance of both single and double-pass SAH. The maximum efficiency of DP-SAH was found to be 63.74% and SP-SAH was found to be 59.62%
Naphon et al. [64]	SHS	Fins	The η_t of the system enhanced as the height and number of fins increases but entropy generation decreases with the increase of the number of fins
Murali et al. [65]	SHS	Fins	The η_t of the air heater when the fins are placed inside the lower channel is more productive or efficiency as compared to the fins embedded inside the upper channel
Singh et al. [66]	SHS	Three types of fins (inline, staggered, and hybrid)	Results showed that a collector with hybrid staggered fins had a thermo-hydraulic efficiency of 79%, which was 13% more efficient than collectors with inline and staggered fins

power with the assistance of the hydro-turbine. In order to enhance the performance and response time of storage systems, advanced PHS systems depend on swapping the turbomachines with reversible pump turbines. A schematic representation of the energy flow in a pumped hydroelectric storage system is shown in Fig. 35.

Compressed air energy storage (CAES)

The CAES system is a process of storing extra energy underground as compressed air. The energy storage procedure starts when the air moves through the compressor. To finish the pressurization, the compression is normally carried out in many phases. Cooling the air happens between each step (intercoolers) and afterward, compression (after cooler), lowering the volume of gas to be stored and also

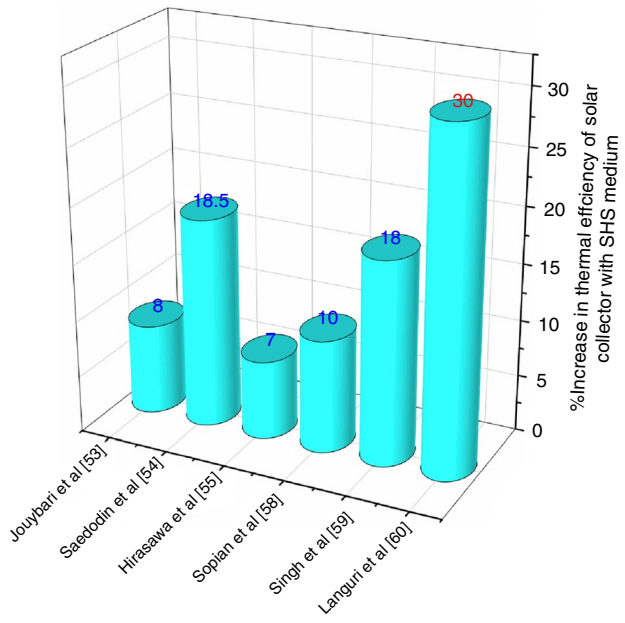

Fig. 31 Efficiency improvement of various STCs with different SHS mediums

removing the heat created during compression. When the process of air compression is finished and the air is stored, it is ready to generate power by releasing the air. During the discharging of air, it is mixed with fuel such as oil and gas and moved through a turbine, where the expansion of air takes place and also releases energy, due to which the turbine starts to spin and thereafter generates electricity with the help of a generator. The hot air from the turbine is frequently sent through a recuperator to exchange heat with compressed air that has recently been released from storage. The schematic diagram of the CAS system is illustrated in Fig. 36.

Olsen et al. [73] presented a new innovative approach and experimental study to harness underground pumped hydroelectric storage. In this PHS system, the mass of the soil is lifted by pumping water into the cavity in the ground to store useful energy. Two impermeable membranes soldered around the edges form the cavity. The results pointed out that the efficiency of the new method is very similar to that of conventional pumped hydroelectric storage. Due to the deformation of the soil, an energy loss of between 0.04 and 0.12% is attained for a system with a power of 30 MW. Li et al. [74] performed a simulated study of molecular dynamics to present a new approach to MES and repossession by utilizing surface energy as a tank in bcc tungsten nanowires, attaining an arrangement of exclusive features, i.e., large actuation stress and strain (>3 GPa, $>30\%$, respectively). Yot et al. [75] directed an experiment to assess the MES performance of aluminum Fumarate material (MOF A520 or MIL-53-FA). The results conclude that MOF A520 or MIL-53-FA materials have been discovered as very capable materials in MES applications as compared to the previously used materials such as porous solids. Tang et al. [76] presented a method by using aligned carbon nanotubes (CNT) with graphene (Ga) pack in sp^2 all- carbon hybrids. It was

Fig. 32 Classification of MES

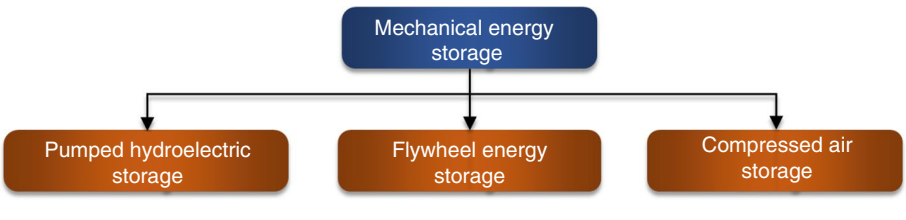

Fig. 33 Different types and shapes of flywheels

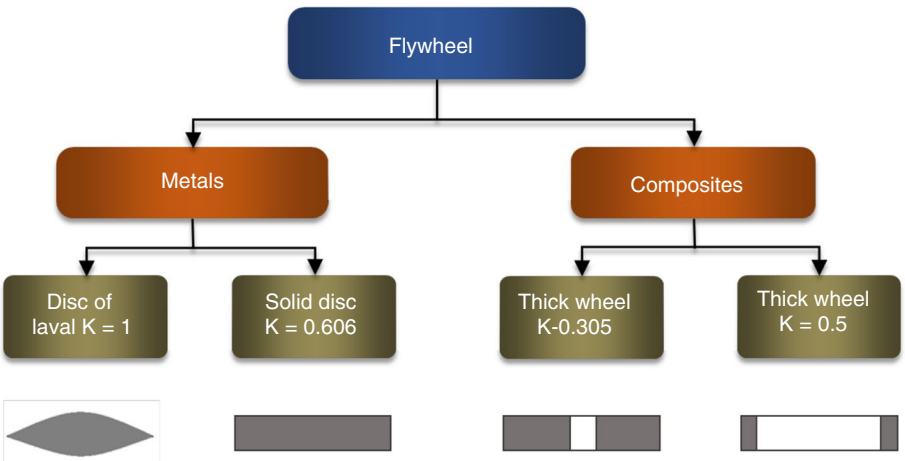

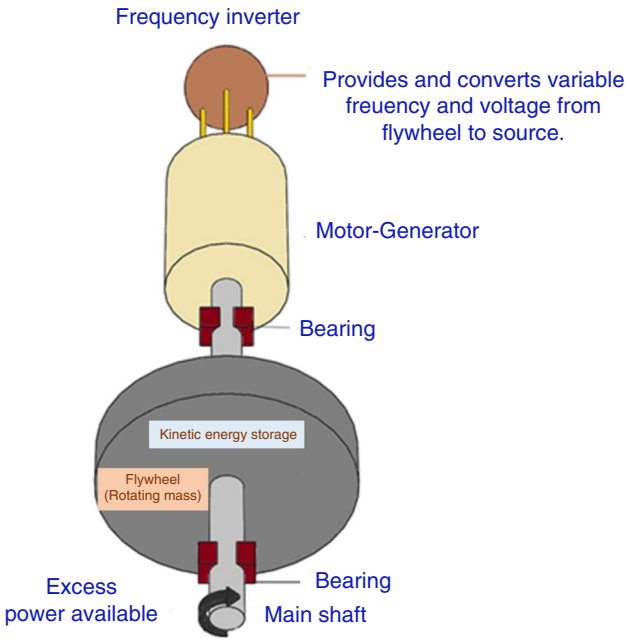

Fig. 34 Different components of flywheel [71]

observed that the CNT/Ga can be compressed at extremely high strains such as ($\mathcal{E} > 90\%$) with high power density and absorption density of 10.4 kW kg^{-1} and 237.1 kJ kg^{-1} and at steady state, the efficiency of these material to store the mechanical energy was found to be 83%. Trinch and Chung [77] examined the morphology impact on the performance of PDMS (polydimethylsiloxane) built on a triboelectric generator (TEG) with an inclined wall array and microtopping (MT).

Electric energy storage (EES)

EES systems are not a recent approach in the area of energy storage and have been used for decades. The EES system involves the storage of electrical energy so that it can be utilized when required.

Electrochemical capacitors

Electrochemical capacitors are characterized by two types: conventional electrostatic capacitors and electrolytic capacitors. The schematic diagram of an electrochemical capacitor is shown in Fig. 37. In orthodox electrolytic capacitors, there are two electrodes placed very close to each other without touching the air or dielectric between the electrodes. Thee plates are then linked to a power source, which creates a voltage between them, making the electrodes oppositely charged (one electrode + ve charged and the other − ve charged). The applied voltage causes the migration of electrons from + vely charged plate toward − vely charged electrode. During this process, one electrode has more electrons than the other electrodes when the power is on. But when power is cut off, the electron moves back to the positive electrode to balance the charge. This tendency of the electron to balance the charge is its potential to do work or store electric energy. On the other hand, electrolytic capacitors are very similar to electrostatic capacitors, but they use an electrolyte in place of one of the electrodes.

The relations below give the amount of energy stored in the capacitor:

$$E = \frac{1}{2}CV^2 \tag{9}$$

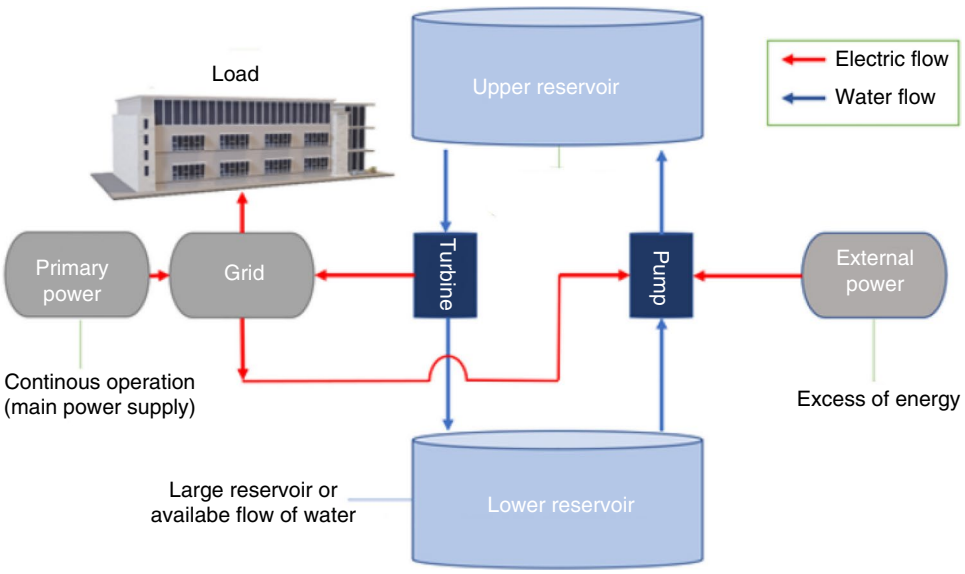

Fig. 35 Schematic illustration of the energy flow in a PHS system [71]

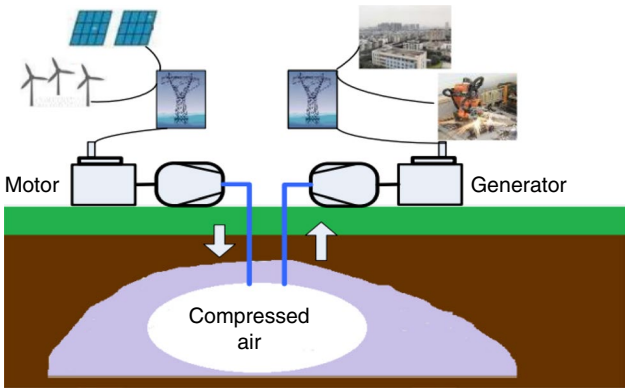

Fig. 36 Schematic diagram of CAS system [72]

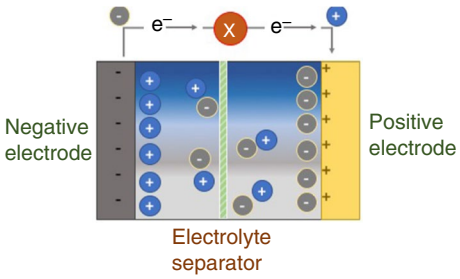

Fig. 37 Schematic diagram of electrochemical capacitor [78]

where V is the voltage applied to the capacitor and C is the capacitance of the device.

Superconducting magnetic energy storage (SMES)

Direct current that passes through the superconducting material does not experience any resistive losses. The current flowing through the coil creates a magnetic field that stores the energy. The DC current moves in a circle indefinitely around the coil until it is required and then discharged. However, there is great feedback from the superconductor that they only work at extremely low temperatures (50–70 °C). These devices need a cryogenic cooling system employing liquid nitrogen or helium, which creates a parasitic energy loss in and of itself. The relations below give the amount of energy stored in the superconductor:

$$E = \frac{1}{2}LI^2 \tag{10}$$

where L is the inductance and I is the amount of current flowing in the superconductor.

Kazempour et al. [79] directed an economic comparative analysis between conventional electric energy storage (EES) and the different developing methods of electric energy storage. A scheduling technique is developed for all EES (both conventional and new) to evaluate their potential for probable profit amid multimarkets like energy, etc. The results showed that investors are most likely to invest in emerging EES systems rather than traditional systems. Schmidtt et al. [80] presented a detailed review paper on photo-rechargeable batteries based on storage modules as well as the solar cells utilized for the EES. It was concluded that solar rechargeable batteries play a significant role in day-to-day life applications such as smart packing. Gagliano and Nocera [81] conducted a performance analysis of EES in residential areas. In this experimental study, the main objective was to recognize or identify energy exchange with a grid of integrated PV-EES systems in very small commercial PV- plants. Li et al. [82] conducted an experimental examination on polyvinylidene fluoride (PVDF) material used for EES. In this experimental work, the investigation of the effect of PVDF crystalline properties on the EES properties was directed. Three distinct crystal structures of PVDF (γ-PVDF, β-PVDF, and γ-PVDF) were investigated. The results pointed out that γ- PVDF can function under a higher electric field and has a maximum energy density of 14 J/cm^3 as compared to γ- PVDF and β-PVDF. Wei and Zhu [83] worked on attaining the very minimum dielectric loss of dielectric polymers and improving the dielectric constant of dielectric polymers so that they can be used for electrical energy storage. It was concluded that dipolar glass polymers are accurate applicants for dielectric polymers that have very low energy loss and have high energy. Guan et al. [84] examined the influence of the crystal orientation of poly (vinylidene fluoride-co-hexafluoropropylene) on the EES capability. The results pointed out that when the PVDF crystals were oriented with c-axes parallel to the electric field, the crystals exhibited low energy density and a low dielectric constant, but when the c-axes were perpendicular to the electric field, a high energy density and a high dielectric constant were achieved.

Biological energy storage (BES)

Two primary forms of energy storage are utilized by living organisms. Energy is stored in the form of covalent chemical bonds within molecules that are particularly rich in energy, such as glycogen and triglycerides. These molecules are created by the cell and then stored away for later use as a source of energy release. The electrochemical form of energy storage is the second most important type of biological energy storage. This form of energy storage manifests itself as gradients of charged ions across cell membranes. Participants are given the opportunity to investigate some of the finer points of energy storage molecules as well as biological energy storage mechanisms that include ion gradients across cell membranes through the use of this educational project.

The utilization of bio-electrochemical devices or bio-batteries based on biological processes will mark a

breakthrough for the electronics sector in generating greener and more sustainable portable energy storage solutions. The ubiquitous usage of cell phones, tablets, and smartwatches has several benefits, including instant access to a vast amount of information and improved interpersonal communication. However, the acquisition of materials required for the manufacture of various gadget components has a negative impact on the environment. Despite the fact that many biological systems are capable of storing energy, the incorporation of biomolecules into energy storage systems (batteries or supercapacitors) is currently uncommon due to their harsh working conditions, which frequently result in the denaturalization of the biological molecules present in the system. Biotechnology and bioengineering could be important players in the creation of batteries and supercapacitors with improved energy and power densities for subsequent generations. Bio-batteries, or bio-electrochemical devices, are energy storage systems that incorporate a bio-based component into their construction. This can be accomplished by imitating naturally occurring solutions, (ii) by changing and adding biological components derived from natural sources (biomaterials), or (iii) by employing biomolecules that can transform substrates into products as shown in Fig. 38 [85].

Biomimetics refers to the practice of emulating natural processes in the development of new products. This solution is based on the observation and research of tactics established by nature during species evolution and applying them to human design issues. One such is the usage of bio-templates, in which living molecules such as viruses serve as scaffolding for the nanoscale synthesis of materials. With the aid of this solution, it is now possible to produce supercapacitor electrodes with greater surface areas using sustainable and effective techniques. We can also discover examples of other biomolecules in this second group, including proteins or fatty acids. Graphene interlayers of supercapacitor electrodes, for instance, were made of conductive graphene, and reduced graphene sheets functionalized with Bovine Serum Albumin (BSA) protein offered nanopores that acted as nanochannels for ions to move between the layers. Although fatty acids are less frequently used for energy storage, their fusion with light-sensitive organic compounds led to the creation of hybrid materials that have the ability to store thermal energy for longer periods of time and release it when an optical trigger is engaged. Last but not least, some systems use bioelectrodes to capture the protons and electrons emitted during the transformation of a substrate into a product. Biofuel cells are the name for these kinds of appliances. Small compounds derived from biomass, such as quinones, flavins, or porphyrins, known for their roles in the electron-transport chain of mitochondria and chloroplasts, can be coupled with cells or enzymes. The second technique entails incorporating biomaterials, which come from biological sources, into energy storage devices. By removing materials from natural sources, this can be accomplished. The most well-known type of compound in this class is a polysaccharide, which can be obtained from fungi, bacteria, or plants. In particular, cellulose has been a separator in batteries since its inception, and it is now widely known for its functions as a binder and a predecessor to carbon electrodes. Frey et al. [86] presented a review of the most current developments in the chemical synthesis and prospective uses of monodisperse magnetic nanoparticles (MFe_2O_4, CoFe, FePt, $SmCo_5$, Co, and Fe). The review goes on to describe these nanoparticles' surface, structural, and magnetic properties for use in magnetic energy storage and biomedicine. Kumar et al. [87] presented a review of the applications of GQD-based materials (Graphene quantum dots) in energy storage. The GQDs and their prospective uses for energy storage systems have all been covered in detail. The use of GQD-based materials application in bio imaging and sensing has been discussed in the article. Gong et al. [88] conducted a study on stiff silkworms made from inexpensive biological waste used as a precursor for the production of well-developed microporous carbon material using carbonization and activation procedures. The results supported the viability of

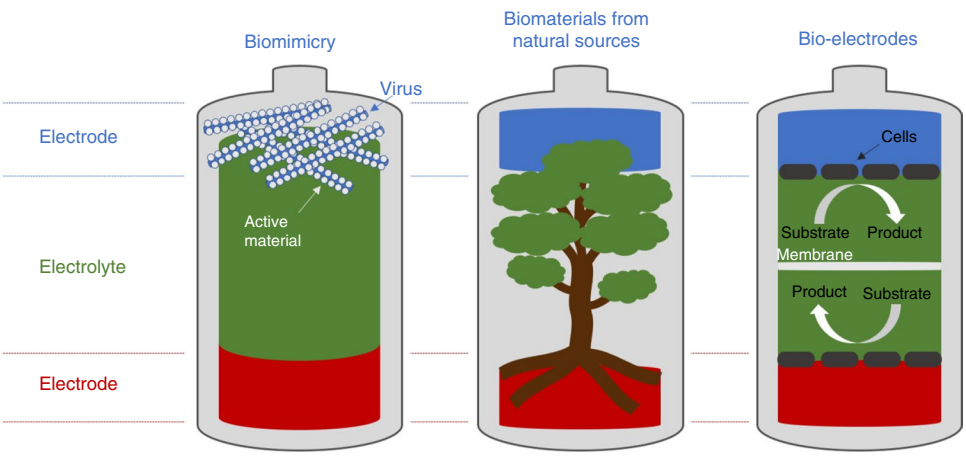

Fig. 38 Different types of methods for the generation of the different biochemical devices and bio-batteries [85]

employing sustainable biomass as a raw material to create high-performance capacitive energy storage devices.

Ayinla et al. [89] presented an overview of the technical developments of the recent palm bio-waste transformation into activated carbon for ES. This review analyzed the pre-treatment conditions, variables for choosing the beginning material, activation methodologies, and activation parameters such as activation temperature, activation time, activation agent, and impregnation ratio. The synergistic effect of palm waste lignocellulose on energy storage was discussed. Salimijazi et al. [90] presented an aggregate performance statistic on the components selected for rewired carbon fixation systems, both biological and non-biological, and the findings pointed out some technical issues and suggested that research work needed to be done in this field.

Chemical energy storage (CES)

Chemical energy storage utilizes the different materials or chemical substances from which energy can be extracted by the different processes of physical sorption, electrochemical sorption, and chemical sorption. Batteries are most commonly used for the storage of chemical energy. The liquid present inside the batteries is used to store the electricity, and this electricity is released when it is required. Electrochemical energy storage batteries have a major role in a wide range of small- and large-scale applications. Large electrochemical batteries can be used by the industry for chemical energy storage. Even the most advanced batteries, such as lithium-ion batteries, have a low volumetric energy density, which is why storing electricity in batteries from solar and wind energy is very challenging. The detailed classification of CES is shown in Fig. 39.

The chemical energy storage principle can be expressed in the form of a reaction:

$$AB + HEAT \leftrightarrow A + B \tag{11}$$

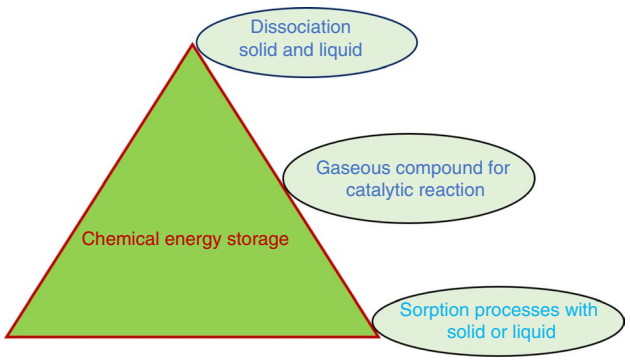

Fig. 39 Classification of CES

Heating of AB compound results in the breaking of AB compound into its components, i.e., A and B, that can be stored separately, and in the reverse process, A and B can both lead to the formation of AB by releasing the heat. The amount of heat used in the given reaction is equal to the storage capacity. The formation of strong or weak bonds can store energy. Materials that involve the formation of strong bonds have better chemical energy storage capacity, i.e., a higher density of energy storage than materials that involve the formation of weak bonds. The materials in which the energy is extracted by the chemical sorption process have a high energy storage density and a low energy storage density when the energy is extracted by the physisorption process. As it is well known, the energy storage capacity of hydrogen is highest, and it can be created or produced from water (H_2O) by going through thermolysis. Thermolysis is a single step of water dissociation. Thermolysis is a very challenging process because it requires a heat source having a high temperature (above 2500 K) for the dissociation of the H_2O and an effective process of separation to avoid a highly reactive mixture of O_2 & H_2.

$$H_2O + HEAT \rightarrow H_2 + 0.5O_2 \tag{12}$$

Over the last few years, major progress has been made in the development of photothermal systems with large-scale solar concentrations (500 W m^{-2}). These solar thermal systems are capable of water thermolysis because of the high temperature of 3000 K of water. The use of the catalyst simplifies the process at a feasible temperature. Two-step thermolysis is more effective than one-step thermolysis, which includes metal oxide for the intermediate redox reaction. Kerskes et al. [91] worked on a four-year research program to examine the technical feasibility of CES for different types of solar thermal applications, as shown in Fig. 40. The reversed solid–gas reaction was used to store the thermochemical energy. The directed research was divided into two aspects: high temperature (> 300 °C) and low temperature (< 100 °C). For the development of compact chemical heat storage for houses, the low-temperature part was utilized, whereas the high-temperature part was used in larger-scale applications such as power plants to store chemical energy with high potential and the ability to increase the energy efficiency of the system. The outcomes showed that the system with CES and vacuum tubes having 6.25 m^3 of storage capacity and 23 m^3 of collector area, respectively, was able to save 50% of the energy of an EnEV house.

Bogdanovic et al. [92] conducted an experimental study by utilizing a reversible metal-hydride-metal system for chemical energy storage. The MgH_2-Mg system was used because of the high energy content of the Mg-H bond and its high temperature-storing capability. The analysis of the results of the high-temperature energy storage when the

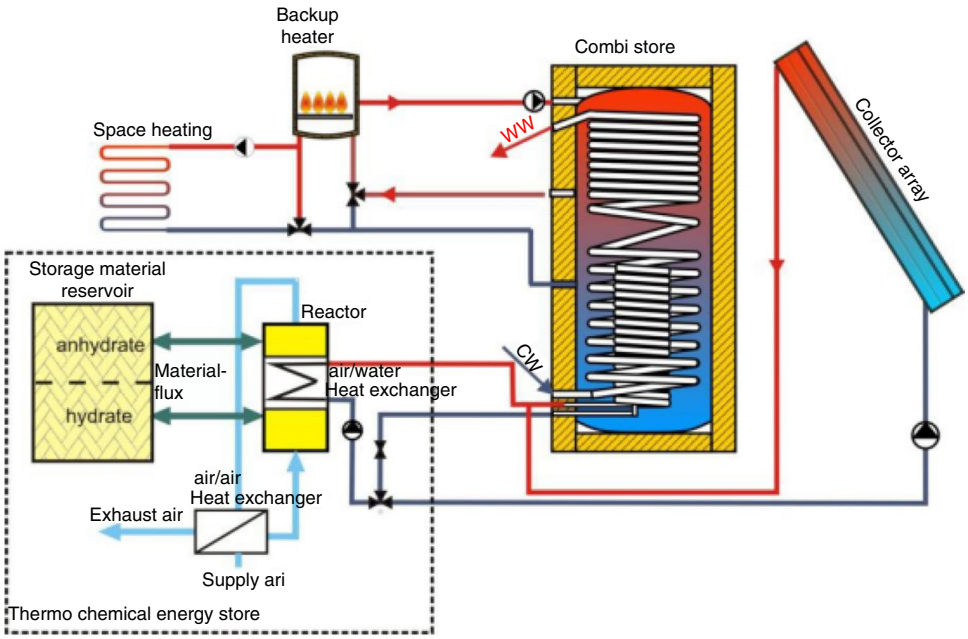

Fig. 40 Schematic diagram of a system using a solar thermal combi system with CES [91]

MgH_2-Mg system was coupled with metal hydride having low-temperature storage ability was conducted.

Murthy et al. [93] presented the decomposition of the calcium hydroxide $Ca(OH)_2$ and experimentally examined the application of Ca $(OH)_2$ for CES. Certain additives such as Ni, Zn, and Al were doped into $Ca(OH)_2$ and the effect of these additives was investigated. The results showed that integration of these additives into $Ca(OH)_2$ improved the reaction rate but the decomposition temperature was significantly dropped. Rauchle et al. [94] led a comparative study between the utilization of methane and methanol synthesized from CO_2 for a better electrochemical energy storage system. The results pointed out that methanol has a better overall efficiency of 49% as compared to methane. The outcomes revealed that gas turbine engines with methanol have a 9% better efficiency rate than methane.

Chadda et al. [95] directed the cyclic reaction of cupric oxide and cuprous oxide (CuO-CuO_2) and examined the potential of the cyclic reaction used for electrochemical energy storage. Scanning electron microscope (SEM) diagrams of surface structures for the 0th and 2nd cycle of CuO/CuO_2 are illustrated in Fig. 41a and surface structures for the 5th and 20th cycle are depicted in Fig. 41b. The obtained results pointed out that up to 20 cycles, the reactivity of the reaction remained unchanged, and due to this CuO–CuO_2 was found to be a good potential entrant for CES.

Lass-Seyoum et al. [96] reported an analysis of the creation of a thermochemically efficient and effective energy storage system (ESS) for use in heating systems and large-scale industrial systems or processes. The new heat exchanger configuration's findings showed a power rate that was 60% greater in bulk than that of the traditional heat exchanger. Brown et al. [97] examined the feasibility of utilizing the CES at the SEG (solar-energy generation) power plants. The reactor heat exchangers schematic diagram is shown in Fig. 42. The revealed that results show that a system built on reversible reaction such as $CaO + H_20 = Ca(OH)_2$ reversible reaction, could be precisely and economically viable for the SE generation at power plants.

Angerer et al. [98] presented an innovative design of a MW-scale CES reactor, as shown in Fig. 43. The main focus was to develop an easy and scalable rector that can be appropriate for industry-scale applications. The achieved results demonstrated that a reactor capacity of 100 m^3 may be used to estimate thermal power of 15 MW using the designed model. Over the years, numerous researchers have worked on developing the various ways for the CES, as described in Table 5.

Artificial energy storage: photonic conversion methods

Combined electrochemical electric energy storage and chemical fuel generation

Electrochemical energy storage (EES) systems are critical to the advancement of sustainable energy technologies. The electric energy produced from various renewable resources, such as solar and wind energy, has a lot of potential to fulfill the energy in a long-term way. Though efficient and consistent electrochemical energy storage (EES) systems are required to store the energy because the electricity generated by utilizing solar or wind energy is very intermittent, as a result, the advancement of new ESS systems is essential to the utilization of large-scale solar and wind-based electricity

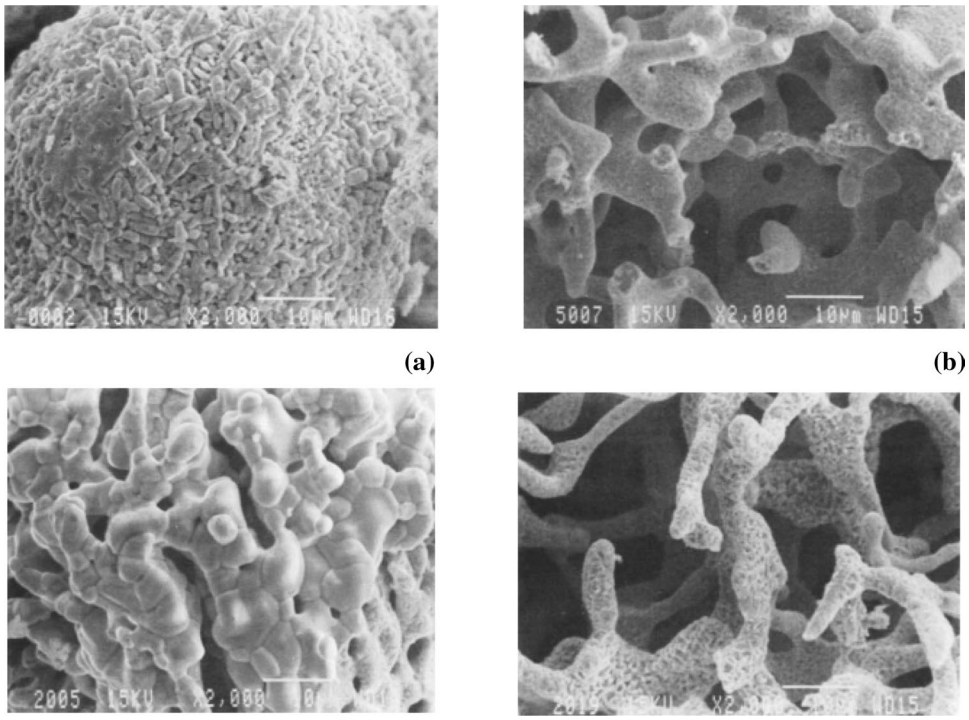

Fig. 41 SEM diagrams: **a** Surface structures for the 0th and 2nd cycle of CuO/CuO_2, **b** Surface structures for the 5th and 20 th cycle [95]

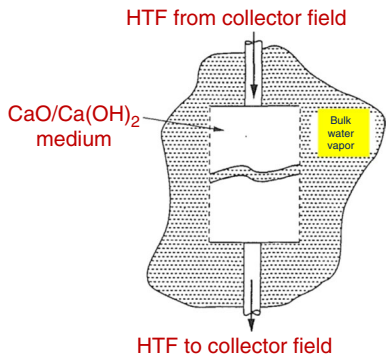

Fig. 42 Reactor heat exchangers [97]

production. The electrical energy produced by the solar cells can be stored, which is the most appropriate way for energy storage. The energy can be stored by using a rechargeable battery, which is the most conventional method of converting electrical energy into chemical energy. Lead-acid batteries are the first rechargeable batteries that were invented by a French scientist in 1859. Pb-acid batteries have a low energy density as compared to modern rechargeable batteries. Sulfuric acid (H_2SO_4) acts as an electrolyte, and the Pb and PbO_2 are the electrodes.

The overall reaction of lead acid batteries is given as:

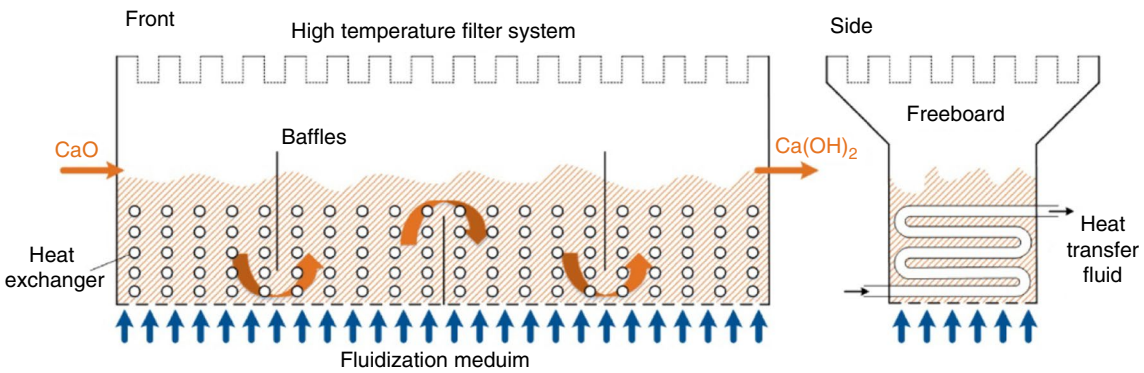

Fig. 43 Reactor design of a continuous MW-scale CES reactor [98]

Table 5 Various experimental studies utilizing different types of techniques for CES

Author	Type of energy storage	Method	Results
Kerskes et al. [91]	CES	Solid–gas reverse reactions	The operating system with CES is able to save 50% of the energy of an EnEV house
Bogdanovic et al. [92]	CES	MgH_2-Mg storage system	An initial temperature increase of 49 K in the low-temperature metal hydride container leads to an upgrading of high-temperature heat in the magnesium container of 23 K
Murthy et al. [93]	CES	$Ca(OH)_2$ with Ni, Zn and Al additives	Integration of additives into $Ca(OH)_2$ improved the reaction rate but the decomposition temperature was significantly dropped
Rauchle et al. [94]	CES	Methane and Methanol	Methanol has a better overall efficiency of 49% as compared to methane and gas turbine engine with methanol has a 9% better efficiency rate than methane
Chadda et al. [95]	CES	CuO/Cu_20	Up to 20 cycles the reactivity of the reaction remained unchanged and due to this $CuO\text{-}CuO_2$ was found to be a good potential entrant for CES
Lass-Seyoum et al. [96]	CES	–	The performance of the new heat exchanger configuration illustrated a 60% higher power rate than the conventional heat exchanger in bulk
Brown et al. [97]	CES	–	Economically feasible for the SE generation at power plants
Angerer et al. [98]	CES	–	Utilizing the designed model, a thermal power of 15 MW can be estimated from a reactor volume of 100 m^3

$$PbO_2 + Pb + 2H_2SO_4 \underset{\text{discharging charging}}{\Longleftrightarrow} 2PbSO_4 + 2H_2O \tag{13}$$

Reaction at the negative terminal:

$$Pb + SO_4^{2-} \underset{\text{discharging charging}}{\Longleftrightarrow} PbSO_4 + 2e^- \tag{14}$$

Reaction at the positive terminal:

$$PbO_2 + SO_4^{2-} + 4H^+ + 2e^- \underset{\text{discharging charging}}{\Longleftrightarrow} PbSO_4 + 2H_2O \tag{15}$$

It is clear from Eq. (15) that lead sulfate crystals are formed at both the negative and positive terminals during the discharging process of batteries, and due to the variation in charge on lead, the electrons are released. Whereas in the charging reaction, the lead sulfate is converted into lead at the negative electrode and lead to lead oxide at the positive electrode. Most lead-acid batteries are used in the automobile sector as SLI (starting, lighting, and ignition) batteries because they have high efficiency and are extremely reliable. But these batteries also have some drawbacks, such as a short lifetime and low energy density. They also have poor performance at very low temperatures. Lithium-ion batteries are modern technology rechargeable batteries that utilize the Li ions as a significant component in electrochemistry. Lithium salts thawed in the organic solvent are used as electrolytes. Graphite materials are utilized as anodes, and Li metal oxides ($LiCoO_2$, $LiMO_2$, and $LiNiO_2$) act as cathodes. During the discharging process, ionization of the Li atom takes place at the anode, i.e., it is detached from its electrons. Then these ions of Li pass through the anode and pass through the electrolyte, where they are then re-joined with their electrons at the cathode and neutralized. The schematic diagram of a Li-ion battery is shown in Fig. 44. Li-ion batteries have greater energy density, and their energy density is enhanced up to 200 h kg^{-1} over time. Li-ion batteries are very consistent in electronic applications such as mobile phones, laptops, and smart electrical appliances.

In redox-flow batteries (RFBs), the oxidation and reduction reactions take place and store the energy in the electrolyte of the battery. The oxidation reaction takes place on the anode, and an electron of high potential is released during the discharging process. Further, this electron is passed through the circuit to do the necessary work. This electron now has a low energy potential, which is then accepted by a reduction reaction that takes place at the cathode. During the charging process, the direction of current is reversed, and chemical reactions are also reversed. RFBs are very popular and most capable of storing energy among various electrochemical storage techniques. RFB has a long lifetime and high energy storage density. The schematic view of redox-flow batteries is shown in Fig. 45. The scope of the use of various rechargeable batteries in the growing requirements of the modern world is shown in Fig. 46.

Yoo et al. [102] presented a review of Li-ion battery technology, investigating its rightness for electronic vehicle applications. In the review of the different batteries, such as magnesium batteries, that have electrochemical energy storage and have the application of load leveling,

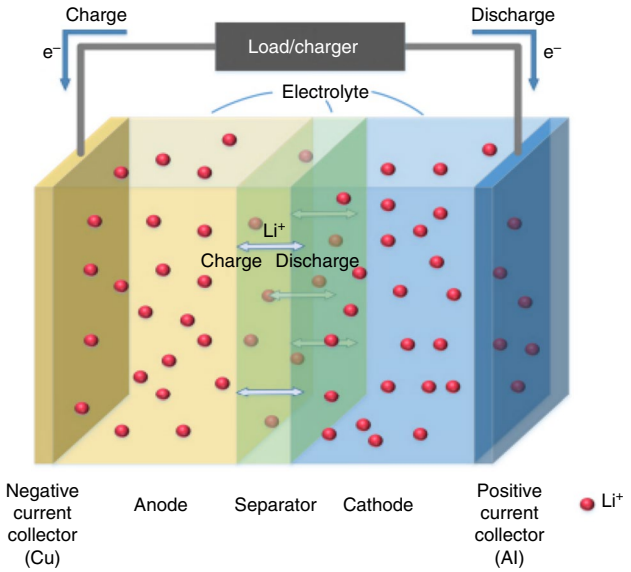

Fig. 44 Schematic diagram Lithium-ion battery [99]

The summarized review of the recent development of various technologies apart from Li-ion, Li–S, and Li–O battery systems was presented. Mathis et al. [103] presented a technique to report the energy storage data in perspective or in an organized way by clarifying the main reasons for incorrect data reporting. The discussion of appropriate and suitable techniques to measure and report metrics such as energy efficiency, capacitance, capacity, power density, and energy density of materials was presented. Hou et al. [104] studied the key characteristics of a flexible electrochemical storage system (ESS) with a hybrid system of electrode materials. The various aspects, classification, and design recommendations of flexible ESS were reported. The viewpoint on current impediments and the applied application of flexible ESS was discussed in this review. Zou et al. [105] analyzed the different prelithiation & presodiation approaches for advanced ESS and summarized their applications such as regeneration or rechargation of used batteries, separator optimization, etc. The future scope of prelithiation & presodiation approaches for the formation of advanced ESS was presented. As it is well known, energy storage batteries or devices exhibit low energy storage density when integrated with photovoltaic cells. Hence, these techniques are not suitable for long-term operations and large energy storage. New techniques are also been developed for the direct conversion of SE into electrical energy without using the photovoltaic cells. For the first time Li–S, the battery is used to directly store the SE when Pt/CdS photocatalyst is introduced into an aqueous polysulfide cathode, and the specific capacity was found to be 4–5 times higher than the conventional Li-ion battery [106]. S^{2-} ions formed during the discharging process and these ions are further oxidized by photoexcited holes of photocatalyst (Pt/CdS) to polysulfide ion. After 2 h

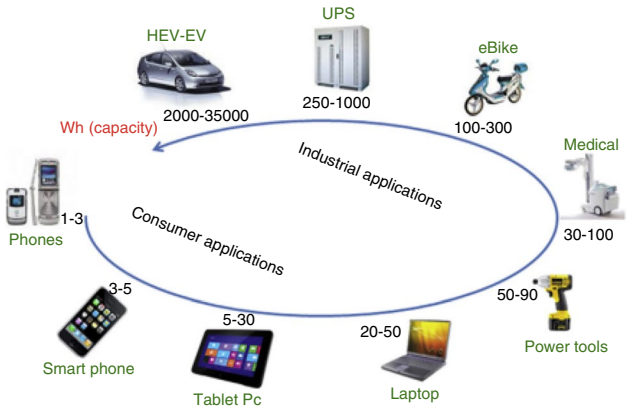

Fig. 46 Scope of use of rechargeable batteries [101]

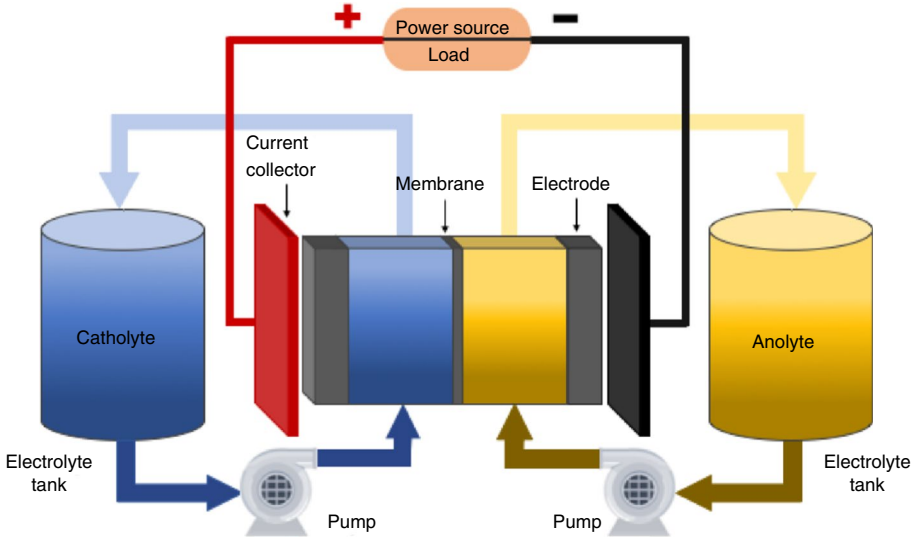

Fig. 45 Schematic view of redox-flow batteries and reactions [100]

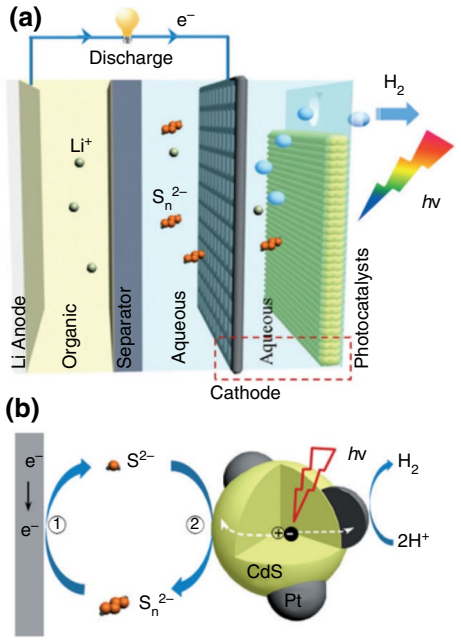

Fig. 47 Schematic diagram of Li–S battery with photocatalyst [107]

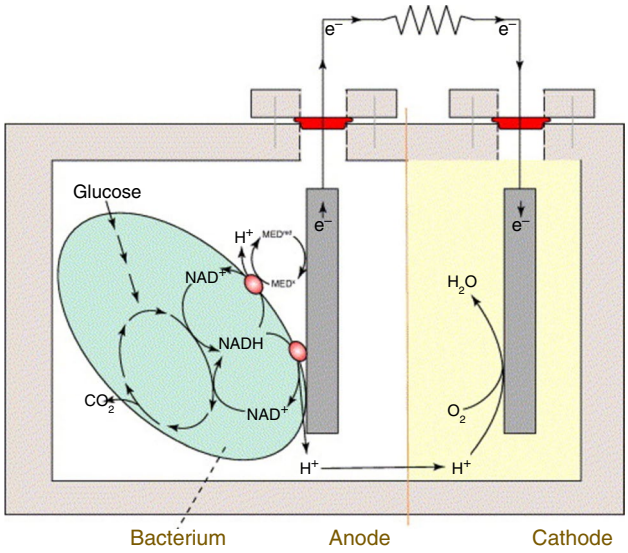

Fig. 48 Schematic diagram and working principle of MFCs [108]

of solar irradiation, Li- S was found to provide a specific capacity of 792 $mAhg^{-1}$. The device is able to simultaneously realize both chemical fuel conversion of SE and electrochemical storage is its most significant advantage. The schematic diagram of the Li–S battery is depicted in Fig. 47 [107].

The reactions are given as follows:

$$\text{Discharge} S_n^{2-} + (2n-2)e^- \rightarrow nS^{2-} \quad (16)$$
(1)

$$\text{Photocatalyst} \xrightarrow{hv} h^+ + e^- \quad (17)$$
(2)

$$nS^{2-} + (2n-2)h^+ \rightarrow S_n^{2-} \quad (18)$$

$$2H^+ + 2e^- \rightarrow H_2 \quad (19)$$

Rabaey et al. [108] presented a study on microbial fuel cells formed from biodegradable compounds, a novel method for the generation of energy. The working principle of MFCs is depicted in Fig. 48. MFCs use the various carbohydrates and substrates of wastewater to function. The anode was used as an elector acceptor by bacteria, and their ability to produce electrical output was examined.

Wang et al. [109] conducted experimental research on solar-assisted MFCs used for the production of bioelectricity and their applications in chemical fuel generation. A schematic and pictorial picture of a conventional MFC with an air cathode is demonstrated in Fig. 49. SE was captured and used to produce bioelectricity and enable the production of hydrogen. The outcomes revealed that solar-MFCs presented the new prospect that these systems are capable of recovering chemical energy from wastewater for CFC generation.

Mohan et al. [110] investigated the bioelectricity production from the treatment of chemical wastewater in MFCs having two chambers, anode and cathode, and injected with H_2 to generate a mixed culture under an acidophilic environment, as illustrated in Fig. 50. The obtained experimental outcomes suggested that the generation of bioelectricity is dependent on substrate loading rate. The results showed that 271.5 mV and 304 mV of maximum voltage were attained at 1.165 kg COD m^{-3} day and 1.404 kg COD m^{-3} day at the operating organic rate.

Hwang et al. [111] examined the influence of the structure of large-area nanotubes/fuels on the production of energy from thermopower waves. The effect of diverse designs, such as 1D CNT arrays, 2D CNT films, and 3D CNT clusters, on the generation of energy was investigated. The findings indicated that designing optimum composites of nanomaterials and fuels, particularly those based on an internal alignment of the materials, can benefit from an understanding of the effects of structure on energy generation from thermopower waves. Safdar et al. [112] presented their study on microfluidic-based fuel cells utilized for the generation of energy. Microfluidic-based cell is far better than conventional fuel cells because they are cost-efficient and has a higher surface area to volume ratio. A brief study on the latest advancement that uses the microfluidic fuel cell potential for the generation or production of energy was presented. Over the years, various researchers worked on developing various methods for electrochemical energy storage as presented in Table 6.

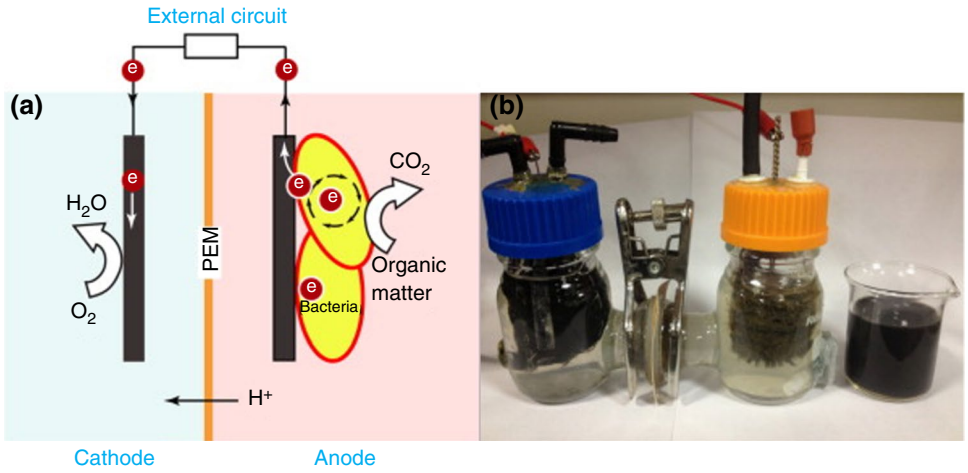

Fig. 49 Schematic and pictorial picture of a conventional MFC with an air cathode [109]

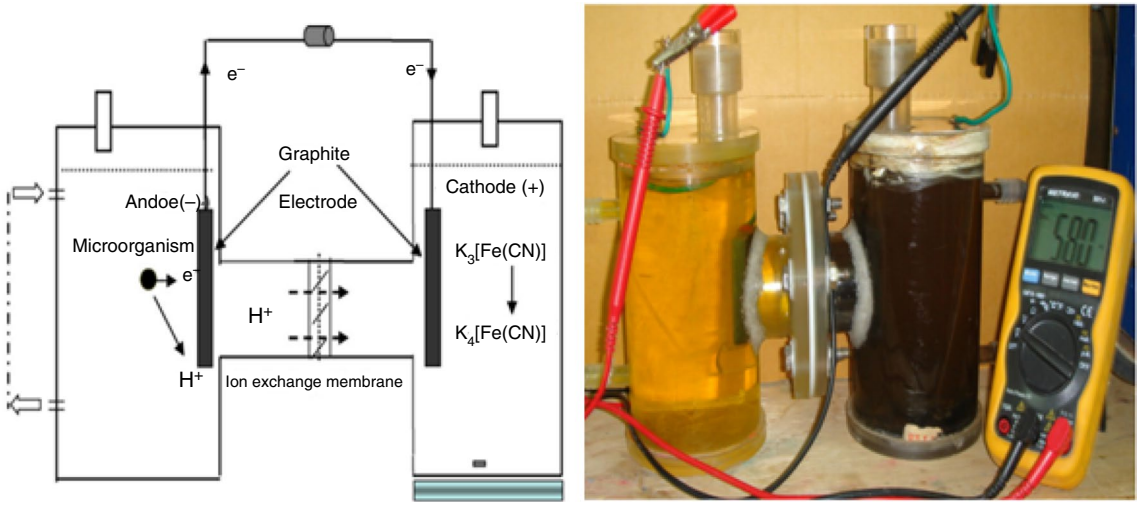

Fig. 50 Graphical details and pictorial view of dual-chambered MFC [110]

Table 6 Various experimental studies have utilized different types of methods for electrochemical energy storage

Author	Type of energy storage	Method	Results
Yoo et al. [102]	EES	Li-ion batteries technology	Presented a brief study of different batteries such as magnesium batteries that has electrochemical energy storage and has application in load leveling application
Zou et al. [105]	EES	Used prelithiation and presodiation approaches	Presented the future scope of prelithiation & presodiation approaches for the formation of advanced ESS
Rabaey et al. [108]	Fuel cell	Microbial fuel cells formed from biodegradable compounds (MFCs)	Investigated how the anode is used as an elector acceptor by bacteria and examined their ability to produce electrical output
Wang et al. [109]	Fuel cell	Microbial fuel cells	Solar-MFCs presented the new prospect that these systems are capable of recovery of chemical energy in wastewater for CFCs generation
Safdar et al. [112]	Fuel cell	Microfluidic-based fuel cell	Presented a brief study on the latest advancement that uses the microfluidic fuel cell potential for the generation or production of energy

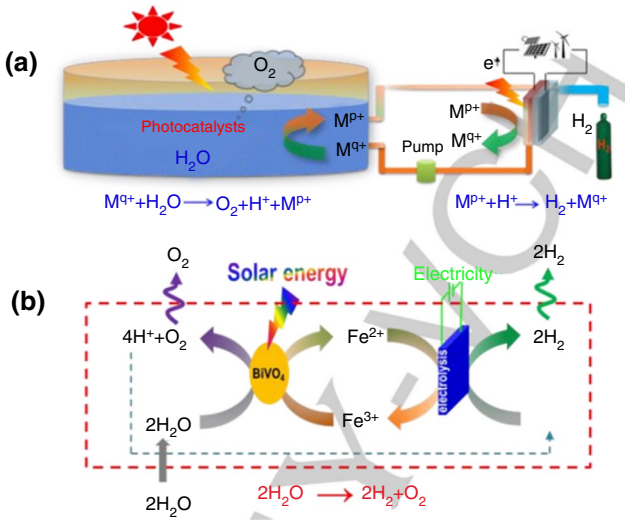

Fig. 51 Schematic diagram of hydrogen production by oxidation of H_2O by using a catalyst [115]

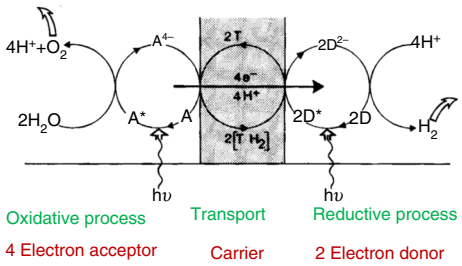

Fig. 52 Schematic representation of a membrane-separated photochemical water splitting system [118]

Storage of SE through hydrogen (H_2) production

Across various fuels, H_2 has among the greatest specific energy densities at 140.4 MJ kg^{-1} (compared to 43.6 MJ kg^{-1} for CH_4), which is one of the benefits of this substance for storing high-density energy. There are several techniques for producing H_2, including the absorption of solar photons, which drives a chemical process during which water splits into H_2 and O_2, a process known as artificial photosynthesis. Photon energy is preserved as chemical energy in a high-energy H_2 product using this technique, which can be performed in several ways. [113, 114]. Zhao et al. [115] worked on hydrogen production by splitting the water by utilizing a suitable photocatalyst, as depicted in Fig. 51. The Hydrogen farm project technique was used in which the SE was captured and Fe3 + /Fe2 + ion loop was incorporated into the hydrogen production system. The results revealed that

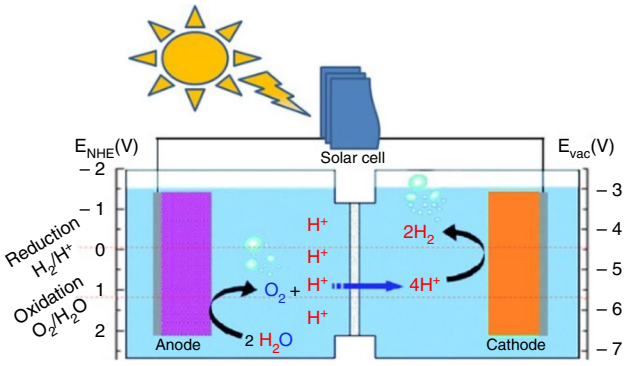

Fig. 53 The main scheme for producing hydrogen in a photovoltaic system with an electrolyzer [20]

overall solar-to-chemical and solar-to-hydrogen efficiency over 1.9% and 1.8% could be attained.

Kubas et al. [116] presented a study on the activation of hydrogen on organometallic complexes and dihydrogen generation and utilization to store energy in the coming years. The generation of hydrogen from water by utilizing SE was of high energy, and its future scope is compared to the existing conventional hydrogen production from natural gas in this review. Singliar et al. [117] presented a brief review of hydrogen production using SE. The review reports on the recent advancements, recommendations, and achievements in the hydrogen production and research areas of photovoltaic cells. Kirch et al. [118] presented a study for hydrogen generation from an aqueous solution of metal complexes by utilizing visible-light irradiation. A schematic representation of membrane-separated photochemical water splitting is demonstrated in Fig. 52. The optimum condition for effective hydrogen generation and the influence of the concentration of the components have been examined.

Photovoltaic (PV) cells with an electrolyzer

This is undoubtedly one of the most advanced choices at the moment, as silicon photovoltaic cells regularly attain efficiencies of more than 15% and electrolyzers frequently attain efficiencies of more than 75%. There is a lot of crucial research being done to enhance the efficiency of PV cells. However, more research is required to investigate the unique demands of a coupled photovoltaic cell with an electrolyzer system. PV-electrolysis methods generate hydrogen by electrolyzing water to create H_2 and O_2 utilizing electrical energy provided by traditional PV cells, as shown in Fig. 53. Just at the anode, two molecules of H_2O are oxidized to produce an O_2 molecule plus four protons that travel across a membrane to the cathode and are converted into two H_2 molecules [119]. Therefore, water electrolysis involves two types of reactions: the oxidation of water at an anode and the reduction of proton at a cathode.

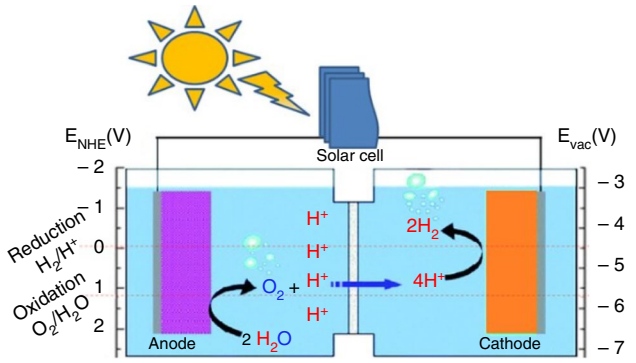

Fig. 54 The basic design for H_2 production in a PEC system includes an *n*-type semiconductor photoanode that evolves O_2 and a photocathode (often a Pt sheet) that evolves H_2 [20]

Overall reaction

$$H_2O \rightarrow H_2 + \left(\frac{1}{2}\right)O_2, \Delta G_0 = 237\frac{kJ}{mol} \tag{20}$$

At anode

$$2H_2O \rightarrow O_2 + 4H^+ + 4e^-, E_0 = 1.23V \tag{21}$$

At cathode

$$2H^+ + 2e^- \rightarrow H_2, E^0 = 0V \tag{22}$$

Solar-to-hydrogen (STH) performance is determined by the performance of a PV cell as well as the performance of an electrolyzer, which frequently surpasses fifty percent [120]. However, the results of early simulation studies on a PV-electrolyzer device that concentrated on silicon PV cells showed that the total performance for H_2 evolution from water could not exceed 4% [121]. It was discovered some time ago that a system consisting of two polymer electrolyte membrane electrolyzers connected in series with a single InGaP/GaAs/GaInNAsSb triple-junction solar cell, which generates a large enough voltage to move both electrolyzers without the need for additional energy input, achieves a 48-h average STH performance of 30%. [122].

Photoelectrochemical cells (PECs) with one or more semiconductor electrodes

Devices that use photoelectrochemical processes typically have two electrodes, an anode, and a cathode, both of which are semiconductors that absorb light, as shown in Fig. 54.

For such type of cell, a semiconductor element is applied as the photoanode to oxidize H_2O, releasing O_2; electrons emitted from the anode are carried by a wire toward a metal cathode (often a platinum electrode), releasing H_2. Despite the fact that the cell generates hydrogen and oxygen without bias, the cell can somehow be classified as chemically biased since the pH in the anode and cathode sections can be considerably distinct. In order to induce photodissociation of H_2O without any applied external potential, semiconductors must meet various energy criteria. Firstly, the semiconductor band gap should be greater as compared to the energy needed for the reaction (i.e., 1.23 eV), however, it should be at least 1.7 to 1.9 eV to compensate for excess potential losses [123]. Secondly, the electron-rich as well as hole-rich species reduction potentials should be adequate to stimulate the appropriate reduction as well as oxidation reactions, respectively; this implies that the semiconductor's conduction band lowest value must be greater than − 0.41 V & its valence band highest should be less than + 0.82 V w.r.t Normal Hydrogen Electrode (NHE) at pH 7 [124]. For the reduction processes to compete with electron–hole recombination, their rates must be fast enough. Just a small number of inorganic semiconductor materials, like SiC (silicon carbide), CdS (cadmium sulfide), CdSe (cadmium selenide), GaP (gallium phosphide), etc., satisfy the above criteria. Whereas cells relying on n-CdS or n-TiO_2 photoanodes illustrated efficiencies of approximately less than ten percent, cells relying on a p-InP photocathode, with small islands of platinum stored, illustrated efficiencies of up to thirteen percent, and those relying on TiO_2 nanotubes illustrated efficiencies of more than sixteen percent [123, 125]. Fewer solar-energy systems with different storage technologies are found easily in various applications [126–140].

Photobiological systems

Such systems generate fuel by fermenting organic substances and converting them to biological hydrogen. Various bacteria, including microalgae, Escherichia coli, and Rhodobacter sphaeroides, have exhibited this capacity [126]. Such systems have the unique benefit of self-assembling collector systems. As a result, as long as the cells can be managed to stay safe and feasible for long periods of time, the expenses of these kinds of systems could indeed be very minimal. Even though the manufacturing of reactor systems required to keep the organisms in optimal circumstances may incur significant expenses. Green algae and cyano bacteria are thought to be among the most efficient photobiological systems for the development of H_2 or O_2. Green algae may generate hydrogen following incubation utilizing multi-enzyme systems within anaerobic circumstances via hydrogenase. It is estimated that the initial H_2 and O_2 production efficiency of these dark-adapted algae is close to 12%, but as regular photosynthesis returns, yields decrease [127]. As sulfur levels drop in algae, it has been discovered that the algae switch from conventional photosynthesis, which produces O_2, to an alternative process, which produces

H_2. [128]. Nitrogen-fixing cyanobacteria can generate H_2, which is catalyzed by the nitrogenase enzyme when the bacteria are depleted of nitrogen. It is important to emphasize that bacteria can produce hydrogen in both light and dark environments; the latter don't really need light energy; thus, they may produce hydrogen continuously during the day as well as at night. Merely a few bacteria, like Rhodobacter sphaeroides, can undergo photofermentation to transform tiny molecular fatty acids into H_2 [126]. Even though efficiency of photobiological hydrogen production under optimal circumstances is typically less than ten percent, and a key obstacle is that algal methods saturate at solar irradiances greater than 3 mW/cm^2, it has already been recommended that biological hydrogen can indeed be developed at commercial level in bioreactors that are using feedstocks; with waste streams is perhaps the most familiar feedstock. As a result, genetic engineering will indeed be needed to decrease the antenna chlorophyll pool size in order to utilize better irradiances. Greenbaum et al. [129] make clear that greater efficiencies (possibly expected to reach 15–20%) may indeed be feasible in specific mutants of Chlamydomonas reinhardii algae lacking Photosystem I.

Combining carbon supplies (succinate, malate) with distinct nitrogen supplies (yeast extract, glutamate) and various metal ions (iron, nickel, magnesium) may regulate the production of hydrogen [126]. The procedure includes feeding bacteria on hydrocarbons as well as removing H_2 and CO_2, in which CO_2 is effectively sequestered by distinct techniques, leaving the H_2 gas.

Photo electrocatalytic systems

Such systems integrate photoelectrochemical and photobiological characteristics by employing enzyme-like catalysts to allow H_2 production under light circumstances as well as an applied bias. This type of system, which is made up of a titanium dioxide (TiO_2) layer on top of functionalized multi-walled carbon nanotubes (CNTs), can be thought of as a three-dimensional electrocatalytic interface. [130]. In a multilayer configuration of Indium Phosphide Quantum Dots activated by a synthetic iron-sulfur electrocatalyst connected to the FeFe-hydrogenase subsite, Nann et al. [131] established a new nano-photocathode for H_2 generation. The researchers were successful in achieving a photoelectrochemical efficiency of greater than sixty percent.

Photodegradation systems

Such systems offer another method for producing solar hydrogen that does not require the evolution of O_2. Organic compounds are employed as consumables in this scenario of a reduction-half reaction. As an example, consider the reaction:

$$CH_3COOH(aq.) + O_2 \rightarrow 2CO_2 + 2H_2 \quad (23)$$

The exergonicity and fuel value of the produced H_2 from this reaction are 392.3 kJ and 474 kJ respectively. The process involves transforming the organic fuel CH_3COOH (Acetic Acid), which has an energy content of 866 kJ into another fuel ($2H_2$, with an energy content of 474 kJ). But if the organic material is a pollutant, hydrogen generation is an excess that only happens when a pollutant is eliminated, and the sunlight is used in this process to oxidize organic pollutants to carbon dioxide and water. But dual-purpose photocatalysis continues to remain a difficult problem. It was discovered that a catalyst plays an important part in the photodegradation method. It has been claimed that in certain circumstances, it should be feasible to generate molecular H_2 from the debasement of organic substances using solar irradiation of the organic substance with the availability of a catalyst, for example, TiO_2 (titanium dioxide) [132], with the typical Eq. (24):

$$C_xH_yO_z + (x - z)\, H_2O \rightarrow xCO_2 + (2x + 0.5y - z)\, H_2 \quad (24)$$

The photodegradation system gains importance by coupling H_2 evolution with the photodegradation of organic contaminants. UV or solar light treatment for organic pollutants in contaminated waterways appears to be highly expensive, with treatment costs ranging between $1 and $50 per kilogram of polluted material cleared. Significant value may be taken into account if H_2 could be developed simultaneously as organic contaminants are photodegraded.

Conclusions

This study is a primary contribution to the examination of the various energy storage methods that are currently in use. Energy storage is undoubtedly expensive, but as we've seen, it's already economical in a lot of situations. As more research and development is done in the sector, more and more application opportunities will become available. The increase in energy demand has pushed the world toward the utilization of non-conventional sources of energy, so technology is required to be developed for the storage of these. SE storage is a very promising approach to preserving energy for long-term and effective consumption. This review paper demonstrated that energy storage can be achieved by utilizing some very basic methods and materials. A comprehensive evaluation of several energy storage techniques is natural energy storage, TES, EES, MES, CES, BES, and ES

using photonic energy conversions. Some of the key findings are highlighted below:

- TES is one of the most promising techniques used for energy storage. TES can be achieved by using LHS and SHS. The efficiency of the various solar collectors was found to be increased by 8–37% by using LHS, and 7–30% was found to be increased by SHS compared with conventional solar thermal collectors.
- The maximum η_t enhancement of 37% was attained by the ETC incorporated by PCM (SA-67) used as LHS medium, whereas the maximum η_t enhancement of 30% was achieved by DP-SAH embedded with porous medium used as SHS medium compared with conventional solar thermal collectors.
- While the process of photosynthesis enables the natural storage of SE, it is important to note that only a fraction of the photons that reach the Earth's surface can be effectively stored. Specifically, the storage capacity is estimated to be around one photon per thousand photons received. This study shows that artificial energy storage techniques are far superior to natural energy storage methods.
- Electrochemical and redox-flow batteries have enhanced efficiency, reaching up to 90% in the field of energy storage.
- Hydrogen energy storage systems have emerged as a prominent category among the diverse range of energy storage systems, exhibiting the potential to induce significant transformations within the existing energy system. There exist various technological, economic, social, and political limitations that must be surpassed prior to the widespread implementation of hydrogen technologies.
- Solar-to-hydrogen efficiency attained up to 10%, 16%, 30%, and 60% in the photobiological system, photoelectrochemical system, PV-electrolysis system, and photoelectrocatalytic system, respectively.
- Investing in research and development to explore the potential of integrating multiple storage techniques with a renewable energy source will optimize the system's overall efficiency and minimize greenhouse gas emissions from conventional gas-burning power plants. With further advancement in energy storage techniques, it is predictable that the cost of kilowatt-hour energy will reduce effectively and will be less than the energy produced or generated by non-renewable sources. With the expansion of these types of energy storage systems, environmental pollution will also decrease, which is caused by non-renewable energy sources (hydrocarbons). Energy storage systems may and must be introduced and actively exploited in both industrial and developing nations' energy policies and technologies.

Acknowledgements The authors extend their appreciation to the Deanship of Scientific Research at King Khalid University for funding this work through large group Research Project under grant number RGP 1/80/44.

Funding Open access funding provided by the Scientific and Technological Research Council of Türkiye (TÜBİTAK).

References

1. Ritchie H, Roser M. Energy production and consumption. Our World in Data; 2019. https://ourworldindata.org/grapher/primary-energy-cons?time=2019.
2. Fahrenbruch A, Bube R. Fundamentals of solar cells: photovoltaic SE conversion. London: Elsevier; 2012.
3. Sherrington C, Moran D. Modelling farmer uptake of perennial energy crops in the UK. Energy Policy. 2010;38:3567–78.
4. Deng YY, Blok K, Van Der Leun K. Transition to a fully sustainable global energy system. Energy Strategy Rev. 2012;1(1):109–21.
5. Steinberger JK, Roberts JT. From constraint to sufficiency: the decoupling of energy and carbon from human needs. Ecol Econ. 2010;70:425–33.
6. Lee CC. The causality relationship between energy consumption and GDP in G-11 countries revisited. Energy Policy. 2006;34:1086–93.
7. Groenemans H, Saur G, Mittelsteadt C, Lattimer J, Xu H. Techno-economic analysis of offshore wind PEM water electrolysis for H_2 production. Curr Opin Chem Eng. 2022;37:100828.
8. Lee B, Lim D, Lee H, Byun M, Lim H. Techno-economic analysis of H_2 energy storage system based on renewable energy certificate. Renew Energy. 2021;167:91–8.
9. Kuravi S. Thermal energy storage technologies and systems for concentrating solar power plants. Prog Energy Combust Sci. 2013;39:285–319.
10. Bhardwaj AK, Kumar R, Chauchan R, Kumar S. Experimental investigation and performance evaluation of a novel solar dryer integrated with a comination of SHS and PCM for drying Chilli in Himalyan region. Therm Sci and Eng Prog. 2020;20:100713.
11. Hadiya J, Shukla AKN. Thermal energy storage using phase change materials: a way forward. Int J Glob Energy Issues. 2018;41:108–27.
12. Abhat A. Low temperature latent heat thermal energy storage: heat storage materials. Sol energy. 1983;30:313–32.
13. Revankar ST. Chemical energy storage. In Storage and Hybridization of Nuclear Energy: Academic Press; 2019. p. 177–227.

14. Sapoznikov D. Mechanism of photosynthesis. Sovetskaya Botanika. 1940;5:93–112.
15. Ross RT, Calvin M. Thermodynamics of light emission and free-energy storage in photosynthesis. Biophys J. 1967;7:595–614.
16. Malkin S. Photochemical energy storage and volume changes in the microsecond time range in bacterial photosynthesis—a laser induced optoacoustic study. J Photochem Photobiol B. 1994;23:79–85.
17. Smil V. Energy in nature and society: general energetics of complex systems. MIT press; 2007.
18. Zhu XG, Long SP, Ort DR. What is the maximum efficiency with which photosynthesis can convert SE into biomass. Curr Opin Biotechnol. 2008;19:153–9.
19. Barber J. Photosynthetic energy conversion: natural and artificial. Chem Soc Rev. 2009;38:185–96.
20. Dimitriev O, Yoshida T, Sun H. Principles of SE storage. Energy Storage. 2020;2:96.
21. De Blasio C. Fundamentals of biofuels engineering and technology. Cham: Springer; 2019.
22. Dimitriev OP. Global energy consumption rates: where is the limit. Sustain Energy. 2013;1:1–6.
23. Zubair S, Pant R. Experimental investigation of solar thermal flat plate collector with and without PCM. Int J Innov Res Sci Eng Technol. 2015;4:2347–6710.
24. Halim A, Jalaluddin AM, Arif E. Performance investigation of solar water heating system integrated with PCM storage. J Mech Eng Res Dev. 2020;43(3):291–300.
25. Murali G, Mayilsamy K, Arjunan TV. An experimental study of PCM-incorporated thermosyphon solar water heating system. Int J Green Energy. 2015;25:978–86.
26. Serale G, Baronetto S, Goia F, Perino M. Characterization and energy performance of a slurry PCM-based solar thermal collector: a numerical analysis. Energy Procedia. 2014;48:223–32.
27. Chopra K, Pathak AK, Tyagi VV, Pandey AK, Anand S, Sari A. Thermal performance of phase change material integrated heat pipe evacuated tube solar collector system: an experimental assessment. Energy Convers Manag. 2020;203:112205.
28. Feliński P, Sekret R. Experimental study of evacuated tube collector/storage system containing paraffin as a PCM. Energy. 2016;114:1063–72.
29. Essa MA, Rofaiel IY, Ahmed MA. Experimental and theoretical analysis for the performance of evacuated tube collector integrated with helical finned heat pipes using PCM energy storage. Energy. 2020;206:118166.
30. Mehla N, Yadav A. Thermal analysis on charging and discharging behaviour of a phase change material-based evacuated tube solar air collector. Indoor Built Environ. 2018;27:156–72.
31. Sudhakar P, Cheralathan M. Encapsulated PCM based double pass solar air heater: a comparative experimental study. Chem Eng Commun. 2021;208:788–800.
32. Baig W, Ali HM. An experimental investigation of performance of a double pass solar air heater with foam aluminum thermal storage medium. Case Stud Therm Eng. 2019;14:100440.
33. Sajawal M, Rehman TU, Ali HM, Sajjad U, Raza A, Bhatti MS. Experimental thermal performance analysis of finned tube-phase change material based double pass solar air heater. Case Stud Therm Eng. 2019;15:100543.
34. Salih SM, Jalil JM, Najim SE. Experimental and numerical analysis of double-pass solar air heater utilizing multiple capsules PCM. Renew Energy. 2019;143:1053–66.
35. Assadeg J, Al-Waeli AH, Fudholi A, Sopian K. Energetic and exergetic analysis of a new double pass solar air collector with fins and phase change material. Sol Energy. 2021;226:260–71.
36. Korti AI. Numerical heat flux simulations on double-pass solar collector with PCM spheres media. Int J Air-Cond Refrig. 2016;24:1650010.
37. Ali HM, Bhatti AI, Ali M. An experimental investigation of performance of a double pass solar air heater with thermal storage medium. Therm Sci. 2015;19:1699–708.
38. Singh AK, Agarwal N, Saxena A. Effect of extended geometry filled with and without phase change material on the thermal performance of solar air heater. J Energy Storage. 2021;39:102627.
39. Srivastava RK, Kumar Rai A, Prasad B. Performance analysis of single pass flat plate recycled SAH integrated with use of thermal energy storage medium. Int J Eng Res Appl. 2020;10:37–42.
40. Ameri M, Sardari R, Farzan H. Thermal performance of a V-corrugated serpentine solar air heater with integrated PCM: a comparative experimental study. Renew Energy. 2021;171:391–400.
41. Wang Z, Diao Y, Zhao Y, Chen C, Liang L, Wang T. Thermal performance of integrated collector storage solar air heater with evacuated tube and lap joint-type flat micro-heat pipe arrays. Appl Energy. 2020;261:114466.
42. Raj AK, Srinivas M, Jayaraj S. A cost-effective method to improve the performance of solar air heaters using discrete macro-encapsulated PCM capsules for drying applications. Appl Therm Eng. 2019;146:910–20.
43. Moradi R, Kianifar A, Wongwises S. Optimization of a solar air heater with phase change materials: experimental and numerical study. Exp Therm Fluid Sci. 2017;89:41–9.
44. Wang TY, Diao YH, Zhu TT, Zhao YH, Liu J, Wei HQ. Thermal performance of solar air collection-storage system with phase change material based on flat micro-heat pipe arrays. Energy Convers Manag. 2017;142:230–43.
45. Alva G, Liu L, Huang X, Fang G. Thermal energy storage materials and systems for SE appl**ic**ations. Renew Sustain Energy Rev. 2017;68:693–706.
46. Allen KG, Von Backström TW, Kröger DG. Packed bed pressure drop dependence on particle shape, size distribution, packing arrangement and roughness. Powder technol. 2013;246:590–600.
47. Abi Mathew A, Thangavel V. A novel thermal storage integrated evacuated tube heat pipe solar air heater: energy, exergy, economic and environmental impact analysis. Sol Energy. 2021;220:828–42.
48. Kumar R, Pathak AK, Kumar M, Patil AK. Experimental study of multi tubular sensible heat storage system fitted with wire coil inserts. Renew Energy. 2021;164:1244–53.
49. Kalaiarasi G, Velraj R, Swami MV. Experimental energy and exergy analysis of a flat plate solar air heater with a new design of integrated sensible heat storage. Energy. 2016;111:609–19.
50. Jain D, Jain RK. Performance evaluation of an inclined multi-pass solar air heater with in-built thermal storage on deep-bed drying application. J Food Eng. 2004;64:497–509.
51. Jain D. Modeling the performance of the reversed absorber with packed bed thermal storage natural convection solar crop dryer. J food Eng. 2007;78:637–47.
52. Kareem MW, Habib K, Ruslan MH, Saha BB. Thermal performance study of a multi-pass solar air heating collector system for drying of Roselle (*Hibiscus sabdariffa*). Renew Energy. 2017;113:281–92.
53. Jouybari HJ, Saedodin S, Zamzamian A, Nimvari ME, Wongwises S. Effects of porous material and nanoparticles on the thermal performance of a flat plate solar collector: an experimental study. Renew Energy. 2017;114:1407–18.
54. Saedodin SA, Zamzamian SA, Nimvari ME, Wongwises S, Jouybari HJ. Performance evaluation of a flat-plate solar collector filled with porous metal foam: experimental and numerical analysis. Energy Convers Manag. 2017;153:278–87.
55. Hirasawa S, Tsubota R, Kawanami T, Shirai K. Reduction of heat loss from solar thermal collector by diminishing natural convection with high-porosity porous medium. Sol Energy. 2013;97:305–13.

56. Kareem MW, Gilani SI, Habib K, Irshad K, Saha BB. Performance analysis of a multi-pass solar thermal collector system under transient state assisted by porous media. Sol Energy. 2017;158:782–91.
57. Roy A, Hoque ME. Performance analysis of double pass solar air heater with packed bed porous media in Rajshahi. AIP Conf Proc. 2017;1851:020010.
58. Sopian K, Alghoul MA, Alfegi EM, Sulaiman MY, Musa EA. Evaluation of thermal efficiency of double-pass solar collector with porous–nonporous media. Renew Energy. 2009;34:640–5.
59. Singh S. Experimental and numerical investigations of a single and double pass porous serpentine wavy wire mesh packed bed solar air heater. Renew Energy. 2020;145:1361–87.
60. Languri EM, Taherian H, Hooman K, Reisel J. Enhanced double-pass solar air heater with and without porous medium. Int J Green Energy. 2011;8:643–54.
61. Sopian K, Daud WR, Othman MY, Yatim B. Thermal performance of the double-pass solar collector with and without porous media. Renew Energy. 1999;18:557–64.
62. Jasim MA. Thermal evaluation of a double-pass unglazed solar air heater with perforated plate and wire mesh layers. Sustainability. 2020;12:3619.
63. Omojaro AP, Aldabbagh LB. Experimental performance of single and double pass solar air heater with fins and steel wire mesh as absorber. Appl Energy. 2010;87:3759–65.
64. Naphon P. On the performance and entropy generation of the double-pass solar air heater with longitudinal fins. Renew Energy. 2005;30:1345–57.
65. Murali G, Nandan BS, Reddy NS, Teja D, Kumar N. Experimental study on double pass solar air heater with fins at lower and upper channel. Mater Today Proc. 2020;21:578–83.
66. Singh S. Thermohydraulic performance of double pass solar thermal collector with inline, staggered and hybrid fin configurations. J Energy Storage. 2020;27:101080.
67. Agrawal P, Gautam A, Kunwar A, Kumar M, Chamoli S. Performance assessment of heat transfer and friction characteristics of a packed bed heat storage system embedded with internal grooved cylinders. Sol Energy. 2018;161:148–58.
68. Lakshmi DV, Layek A, Kumar PM. Performance analysis of trapezoidal corrugated solar air heater with sensible heat storage material. Energy Procedia. 2017;109:463–70.
69. Koekemoer LA. Effect of material type and particle size distribution on pressure drop in packed beds of large particles: extending the Ergun equation. Fuel. 2015;158:232–8.
70. Halkarni SS, Sridharan A, Prabhu SV. Influence of inserts on the pressure drop distribution in randomly packed beds with uniform sized spheres in the endshield model of AHWR. Exp Therm Fluid Sci. 2016;74:181–94.
71. Mahmoud M, Ramadan M, Olabi AG, Pullen K, Naher S. A review of mechanical energy storage systems combined with wind and solar applications. Energy Convers Manag. 2020;210:112670.
72. Wang J, Lu K, Ma L, Wang J, Dooner M, Miao S, Li J, Wang D. Overview of compressed air energy storage and technology development. Energies. 2017;10(7):991.
73. Olsen J, Paasch K, Lassen B, Veje CT. A new principle for underground pumped hydroelectric storage. J Energy Storage. 2015;2:54–63.
74. Li S, Ding X, Li J, Ren X, Sun J, Ma E. High-efficiency mechanical energy storage and retrieval using interfaces in nanowires. Nano lett. 2010;10:1774–9.
75. Yot PG, Vanduyfhuys L, Alvarez E, Rodriguez J, Itié JP, Fabry P, Guillou N, Devic T, Beurroies I, Llewellyn PL, Van Speybroeck V. Mechanical energy storage performance of an aluminum fumarate metal–organic framework. Chem Sci. 2016;7:446–50.
76. Tang C, Zhang Q, Zhao MQ, Tian GL, Wei F. Resilient aligned carbon nanotube/graphene sandwiches for robust mechanical energy storage. Nano Energy. 2014;7:161–9.
77. Trinch VL, Chung CK. Harvesting mechanical energy, storage, and lighting using a novel PDMS based triboelectric generator with inclined wall arrays and micro-topping structure. Appl Energy. 2018;213:353–65.
78. Solomon G, Kohan MG, Landström A, Vomiero A, Concina I. Semiconducting metal oxides empowered by graphene and its derivatives: progresses and critical perspective on selected functional applications. J Appl Phys. 2020;128:180905.
79. Kazempour SJ, Moghaddam MP, Haghifam MR, Yousefi GR. Electric energy storage systems in a based economy: comparison of emerging and traditional technologies. Renew Energy. 2009;12:2630–9.
80. Schmidt D, Hager MD, Schuert US. Photo-rechargeable electric energy storage systems. Adv Energy Mater. 2016;6:1500369.
81. Gagliano A, Nocera F. Analysis of the performances of electric energy storage in residential applications. Int J Heat Technol. 2017;35:S41–8.
82. Li W, Meng Q, Zheng Y, Zhang Z, Xia W, Xu Z. Electric energy storage properties of polyvinylidene fluoride. Appl Phys Lett. 2010;96:192905.
83. Wei J, Zhu L. Intrinsic polymer dielectrics for high energy density and low loss electric energy storage. Prog Polym Sci. 2020;106:101254.
84. Guan F, Pan J, Wang J, Wang Q, Zhu L. Crystal orientation effect on electric energy storage in poly (vinylidene fluoride-co-hexafluoropropylene) copolymers. Macromolecules. 2010;43:384–92.
85. Morant-Miñana M, Biological systems for energy storage solutions, CIC energiGUNE; 2023. https://cicenergigune.com/en/blog/biological-systems-energy-storage-biobatteries.
86. Frey NA, Peng S, Cheng K, Sun S. Magnetic nanoparticles: synthesis, functionalization, and applications in bioimaging and magnetic energy storage. Chem Soc Rev. 2009;38:2532–42.
87. Kumar YR, Deshmukh K, Sadasivuni KK, Pasha SK. Graphene quantum dot based materials for sensing, bio-imaging and energy storage applications: a review. RSC Adv. 2020;10:23861–98.
88. Gong C, Wang X, Ma D, Chen H, Zhang S, Liao Z. Microporous carbon from a biological waste-stiff silkworm for capacitive energy storage. Electrochem Acta. 2016;220:331–9.
89. Ayinla RT, Dennis JO, Zaid HM, Sanusi YK, Usman F, Adebayo LL. A review of technical advances of recent palm bio-waste conversion to activated carbon for energy storage. J Clean Prod. 2019;229:1427–42.
90. Salimijazi F, Parra E, Barstow B. Electrical energy storage with engineered biological systems. J Biol Eng. 2019;13:1–21.
91. Kerskes H, Mette B, Bertsch F, Asenbeck S, Drück H. Chemical energy storage using reversible solid/gas-reactions (CWS)–results of the research project. Energy Proced. 2012;30:294–304.
92. Bogdanović B, Ritter A, Spliethoff B. Active MgH_2-Mg systems for reversible chemical energy storage. Angew Chem. 1990;29:223–34.
93. Murthy MS, Raghavendrachar P, Sriram SV. Thermal decomposition of doped calcium hydroxide for chemical energy storage. Sol Energy. 1986;36:53–62.
94. Räuchle K, Plass L, Wernicke HJ, Bertau M. Methanol for renew energy storage and utilization. Energy Technol. 2016;4:193–200.
95. Chadda D, Ford JD, Fahim MA. Chemical energy storage by the reaction cycle CuO/Cu_2O. Int J Energy Res. 1989;13:63–73.
96. Lass-Seyoum A, Blicker M, Borozdenko D, Friedrich T, Langhof T. Transfer of laboratory results on closed sorption thermochemical energy storage to a large-scale technical system. Energy Proced. 2012;30:310–20.

97. Brown DR, La Marche JL, Spanner GE. Chemical energy storage system for solar electric generating system (SEGS) solar thermal power plant. Int Sol Energy Conf. 1992;114:212–8.
98. Angerer M, Becker M, Härzschel S, Kröper K, Gleis S, Vandersickel A, Spliethoff H. Design of a MW-scale thermo-chemical energy storage reactor. Energy Rep. 2018;4:507–19.
99. Zhang J, Zhang L, Sun F, Wang Z. An overview on thermal safety issues of lithium-ion batteries for electric vehicle application. IEEE Access. 2018;6:23848–63.
100. Clemente A, Ramos GA, Costa-Castelló R. Voltage h∞ control of a vanadium redox flow battery. Electronics. 2020;9:1567.
101. Liu D, Lithium ion battery pack technologies—Li-Ion and LiFePO4 battery pack systems from China manufacturers. JB Battery; 2022. https://www.lithiumbatterychina.com/blog/2019/04/06/lithium-ion-battery-pack-technologies-li-ion-and-lifepo4-battery-pack-systems-from-china-manufacturers/.
102. Yoo HD, Markevich E, Salitra G, Sharon D, Aurbach D. On the challenge of developing advanced technologies for electrochemical energy storage and conversion. Mater Today. 2014;17:110–21.
103. Mathis TS, Kurra N, Wang X, Pinto D, Simon P, Gogotsi Y. Energy storage data reporting in perspective—guidelines for interpreting the performance of electrochemical energy storage systems. Adv Energy Mater. 2019;9:1902007.
104. Hou R, Gund GS, Qi K, Nakhanivej P, Liu H, Li F, Xia BY, Park HS. Hybridization design of materials and devices for flexible electrochemical energy storage. Energy Storage Mater. 2019;19:212–41.
105. Zou K, Deng W, Cai P, Deng X, Wang B, Liu C, Li J, Hou H, Zou G, Ji X. Prelithiation/presodiation techniques for advanced electrochemical energy storage systems: concepts, applications, and perspectives. Adv Funct Mater. 2021;31:2005581.
106. Ji X, Lee K, Nazar L. A highly ordered nanostructured carbon–sulphur cathode for lithium–sulphur batteries. Nature Mater. 2009;8:500–6.
107. Li N, Wang Y, Tang D, Zhou H. Integrating a photocatalyst into a hybrid lithium–sulfur battery for direct storage of SE. Angew Chem. 2015;54:9271–4.
108. Rabaey K, Verstraete W. Microbial fuel cells: novel biotechnology for energy generation. Trends Biotechnol. 2005;23:291–8.
109. Wang H, Qian F, Li Y. Solar-assisted microbial fuel cells for bioelectricity and chemical fuel generation. Nano Energy. 2014;8:264–73.
110. Mohan SV, Mohanakrishna G, Reddy BP, Saravanan R, Sarma PN. Bioelectricity generation from chemical wastewater treatment in mediatorless (anode) microbial fuel cell (MFC) using selectively enriched hydrogen producing mixed culture under acidophilic microenvironment. Biochem Eng J. 2008;39:121–30.
111. Hwang H, Yeo T, Um JE, Lee KY, Kim HS, Han JH, Kim WJ, Choi W. Investigation of the effect of the structure of large-area carbon nanotube/fuel composites on energy generation from thermopower waves. Nanoscale Res Lett. 2014;9:1–9.
112. Safdar M, Jänis J, Sanchez S. Microfluidic fuel cells for energy generation. Lab Chip. 2016;16:2754–8.
113. Steinfeld A. Solar thermochemical production of hydrogen—a review. Sol Energy. 2005;75:603–15.
114. Bolton JR. Solar photoproduction of hydrogen: a review. Sol Energy. 1996;57:37–50.
115. Zhao Y, Ding C, Zhu J, Qin W, Tao X, Fan F, Li R, Li C. A hydrogen farm strategy for scalable solar hydrogen production with particulate photoctalysts. Angew Chem. 2020;132:9740–5.
116. Kubas GL. Hydrogen activation on organometallic complexes and H_2 production, utilization, and storage for future energy. J Organomet Chem. 2009;694:2648–53.
117. Šingliar M. SE using for hydrogen production. Pet Coal. 2007;49:40–7.
118. Kirch M, Lehn JM, Sauvage JP. Hydrogen generation by visible light irradiation of aqueous solutions of metal complexes, an approach to the photochemical conversion and storage of SE. Helv Chim Acta. 1979;62:1345–84.
119. Zhang B, Daniel Q, Cheng M, Fan L, Sun L. Temperature dependence of electrocatalytic water oxidation: a triple device model with a photothermal collector and photovoltaic cell coupled to an electrolyzer. Faraday Discuss. 2017;198:69–179.
120. Pascuzzi S, Anifantis AS, Blanco I, Scarascia MG. Electrolyzer performance analysis of an integrated hydrogen power system for greenhouse heating: a case study. Sustainability. 2016;8:629.
121. Vanhanen J. Simulation of solar hydrogen energy systems. Sol Energy. 1994;53:267–78.
122. Jia J. Solar water splitting by photovoltaic-electrolysis with a solar-to-hydrogen efficiency over 30%. Nat Commun. 2016;7:1–6.
123. Chen HM, Chen CK, Liu RS, Zhang L, Zhang J. Nano-architecture and material designs for water splitting photoelectrodes. Chem Soc Rev. 2012;41:5654–71.
124. Lehn JM. Photo induced generation of hydrogen and oxygen from water in photochemical conversion and storage of SE. In: Proceedings of the 3rd international conference 1981.
125. Paulose M, Shankar K, Yoriya S, Prakasam HE, Varghese OK, Mor GK, Latempa TK, Fitzgerald A. Anodic growth of highly ordered TiO_2 nanotube arrays to 134 μm in length. J Phys Chem B. 2006;110:16179–84.
126. Trchounian A. Mechanisms for hydrogen production by different bacteria during mixed-acid and photo-fermentation and perspectives of hydrogen production biotechnology. Crit Rev Biotechnol. 2015;35:103–13.
127. Greenbaum E. Energetic efficiency of hydrogen photoevolution by algal water splitting. Biophys J. 1988;54:365–8.
128. Hemschemeier A, Melis A, Happe T. Analytical approaches to photobiological hydrogen production in unicellular green algae. Photosynth Res. 2009;102:523–40.
129. Greenbaum E, Lee JW, Tevault CV, Blankinship SL, Mets LJ. CO_2 fixation and photoevolution of H_2 and O_2 in a mutant of Chlamydomonas lacking photosystem. I Nature. 1995;376:438–41.
130. Valenti G. Co-axial heterostructures integrating palladium/titanium dioxide with carbon nanotubes for efficient electrocatalytic hydrogen evolution. Nat Commun. 2016;7:1–8.
131. Nann T. Water splitting by visible light: a nanophotocathode for hydrogen production. Angew Chem Int Ed. 2010;49:1574–7.
132. Kim J, Choi W. Hydrogen producing water treatment through solar photocatalysis. Energy Environ Sci. 2010;3:1042–5.
133. Murugan M, Saravanan A, Elumalai PV, Kumar P, Ahamed Saleel C, Samuel OD, Setiyo M, Enweremadu CC, Afzal A. An overview on energy and exergy analysis of solar thermal collectors with passive performance enhancers. Alex Eng J. 2022;61:8123–47. https://doi.org/10.1016/j.aej.2022.01.052.
134. Felemban BF, Essa FA, Afzal A, Ahmed MH, Saleh B, Panchal H, Shanmugan S, Elsheikh A, Omara ZM. Experimental investigation on dish solar distiller with modified absorber and phase change material under various operating conditions. Environ Sci Pollut Res. 2022. https://doi.org/10.1007/s11356-022-20285-z.
135. El M, Attia H, Driss Z, Elnaby A, Afzal A, Manokar AM, Sathyamurthy R. Phosphate bed as energy storage materials for augmentation of conventional solar still productivity. Environ Prog Sustain Energy. 2021. https://doi.org/10.1002/ep.13581.
136. Prasad AR, El M, Attia H, Al-kouz W, Afzal A, Athikesavan MM. Energy and exergy efficiency analysis of solar still incorporated with copper plate and phosphate pellets as energy storage material. Environ Sci Pollut Res. 2021. https://doi.org/10.1007/s11356-021-14080-5.
137. Akram N, Montazer E, Kazi SN, Soudagar MEM, Ahmed W, Zubir MNM, Afzal A, Muhammad MR, Ali HM, Márquez FPG, et al. Experimental investigations of the performance of a flat-plate solar

collector using carbon and metal oxides based nanofluids. Energy. 2021. https://doi.org/10.1016/j.energy.2021.120452.
138. Huddar VB, Razak A, Cuce E, Gadwal S, Alwetaishi M, Afzal A, Saleel CA, Shaik S. Thermal performance study of solar air dryers for cashew kernel : a comparative analysis and modelling using response surface methodology (RSM) and artificial neural network (ANN). Int J Photoenergy. 2022. https://doi.org/10.1155/2022/4598921.
139. Sheik MA, Aravindan MK, Beemkumar N, Chaurasiya PK, Jilte R, Shaik S, Afzal A. Investigation on the thermal management of solar photo voltaic cells cooled by phase change material. J Energy Storage. 2022;52: 104914. https://doi.org/10.1016/j.est.2022.104914.
140. Nižetić S, Jurčević M, Čoko D, Arıcı M, Hoang AT. Implementation of phase change materials for thermal regulation of photovoltaic thermal systems: comprehensive analysis of design approaches. Energy. 2021;228:120546.